IEEE Access
Multidisciplinary | Rapid Review | Open Access Journal

Received June 23, 2020, accepted July 30, 2020, date of publication August 10, 2020, date of current version August 20, 2020.

Digital Object Identifier 10.1109/ACCESS.2020.3015232

Bivariate Fisher–Snedecor $\mathcal{F}$ Distribution and Its Applications in Wireless Communication Systems

WEIJUN CHENG, (Member, IEEE), AND XIAOTING WANG
School of Information Engineering, Minzu University of China, Beijing 100081, China

Corresponding author: Weijun Cheng (weijuncheng@muc.edu.cn)

This work was supported by the National Natural Science Foundation of China under Grant 61773416.

ABSTRACT Recently, a Fisher–Snedecor $\mathcal{F}$ composite fading model has gained great attention due to its mathematical tractability and modeling accuracy. However, its bivariate statistical characteristics have not been considered yet in the previous technical literature. In this paper, we present a bivariate Fisher–Snedecor $\mathcal{F}$ distribution with identical shaping parameters and study its applications in the wireless communication systems. We first derive novel theoretical formulations of the statistical characteristics for the bivariate Fisher–Snedecor $\mathcal{F}$ distribution model, which include the joint probability density function (PDF), the joint cumulative distribution function (CDF), the joint moment generating function (MGF) and the joint moments. Then, capitalizing on the above statistical expressions, some exact and asymptotic expressions of performance criteria, such as the outage probability, the average bit/symbol error probability (ABEP/ASEP), and the average channel capacity, for dual-branch selection combing and maximal ratio combing diversity systems are derived, respectively. Especially, the exact expressions of the ABEP/ASEP for several classical modulation schemes are obtained in terms of the multivariate Fox's H-function by applying the Mellin-Barnes type contour integral. Furthermore, we investigate the second-order statistics of a sampled Fisher-Snedecor $\mathcal{F}$ composited fading envelope by utilizing the joint CDF, and obtain the mathematical expressions of the level crossing rate (LCR) and the average fade duration (AFD). Finally, we employ numerical and simulation results to demonstrate the validity of the theoretical analysis under various correlated fading and shadowing scenarios.

INDEX TERMS Correlated composite fading, Fisher–Snedecor $\mathcal{F}$ distribution, maximal ratio combing, selection combing, second-order statistics.

I. INTRODUCTION

In many practical wireless environments (e.g., congested downtown areas with slowing moving pedestrians and vehicles), the received signals in the wireless receivers often suffer from multipath fading and shadowing simultaneously [1]. To characterize the composite effect of the multipath fading and shadowing and predict accurately the performance of a wireless communication system, two popular composite fading channel models have been proposed by combining multipath fading with shadowing. One is a multiplicative shadowing model assuming both the dominant components and the scattered waves are shadowed equally, and the other is named as line-of-sight (LOS) shadowing model in which shadowing only affects the dominant components [2]. The Rician shadowed and the κ-μ shadowed models are two typical examples of the latter. In the open technical literature, the multiplicative composite model can be divided into four categories: the lognormal (LN) based model, the Gamma (GA) based model, the inverse Gaussian (IG) based model, and the inverse Gamma (IGA) based model [3], [4]. The LN-based model mainly includes, but is not limited to, Rayleigh-LN, Rice-LN, Nakagami-LN, Weibull-LN, α-η-μ-LN, and α-κ-μ-LN [5]. The common shortcoming of these models is their rather cumbersome mathematical expressions, which make them rather inconvenient to evaluate accurately the performance of wireless communication systems and restrict their potential applications. To avoid this issue, some alternative models had been studied in the past decades. The GA-based model is an earlier substituted version of the former by using GA distribution to replace LN one. So far, the published papers about this model are rather extensive. They include the K distribution (Rayleigh-GA) and its generalized version (Nakagami-GA, hereafter referred to as the KG), Weibull-GA, η-μ-GA, and κ-μ-GA [4]. Since GA distribution is not a good approximation for LN

The associate editor coordinating the review of this manuscript and approving it for publication was Matti Hämäläinen.

distribution with large variance, the third model has been proposed by using the IG distribution to replace GA when a long-tailed behavior is considered. The IG-based model includes Rayleigh-IG [6], Nakagami-m/IG (hereafter referred to as the $\mathcal{G}$ distribution) model [7], Rice-IG [8], η-μ-IG, κ-μ-IG and α-μ-IG [9]. The results investigated in [7] depicted the IG-based model can provide a more accurate approximation for LN distribution and better characterization of fading channels in comparison with the GA-based models. Unfortunately, in order to evaluate the performance of some more complicated wireless communication systems by applying the above models, for example, multipath diversity systems and multi-hop cooperative systems, the mathematical forms of some performance metrics of interest, namely the outage probability (OP) and the average bit/symbol error probability (ABEP /ASEP), still become intractable. To overcome these mathematical difficulties, some further approximations have to be used, such as mixture Gamma distribution [3], [10] and mixture IG distribution [9]. However, these approximated forms ignore modeling accuracy. For this reason, the IGA-based model achieves an appropriate balance between the modeling accuracy and the calculation complexity. In [11], the η-μ-IGA and κ-μ-IGA models not only provided a good fit for modeling the composite fading channels but also can be extended to the conventional and emerging wireless communication systems, such as cellular, wearable, and vehicular wireless applications.

More recently, an alternative version of the IGA-based model, namely the Fisher-Snedecor $\mathcal{F}$ fading channel model, was proposed in [12]. This model is based on the fact that the square root of an inverse gamma random variable follows an inverse Nakagami-m distribution. It accurately describes the composite effects of both shadowing components and multipath components on the fading signal, where shadowing components follow inverse Nakagami-m distribution, and multipath components follow Nakagami-m distribution. Compared to the KG composite fading model, the authors in [12] showed that under non-LOS (NLOS) and LOS environments the Fisher composite fading model has a better fit for experimental channel measurements, such as wireless body area networks and device-to-device (D2D) communications. Furthermore, this fading model can reduce to one-sided Gaussian, Rayleigh, and Nakagami-m in the absence of shadowing components. Importantly, its alternative advantage is that the closed-form expressions of its statistical characteristics are more tractable and simpler than those of KG distribution.

As a result, the performance analysis of wireless digital communication systems over Fisher-Snedecor $\mathcal{F}$ composite fading channels has gained great attention in [13]–[22] and references therein. The authors in [13] gave the theoretical formulations of the sum of independent and non-identically distributed (i.n.i.d.) random variables (RVs) following Fisher-Snedecor $\mathcal{F}$ distribution and applied them in maximal ratio combining (MRC) receivers. The performance of physical layer security was investigated over $\mathcal{F}$ composite fading channels in [14]. The authors in [12] further studied the achievable channel capacity and energy detection-based spectrum sensing in Fisher-Snedecor $\mathcal{F}$ fading in [15] and [16], respectively. In [17], the performance of the selection combining (SC) scheme with i.n.i.d branches over $\mathcal{F}$ composite fading channels was analyzed. Authors in [18] considered the ergodic capacity of several adaptive transmission strategies and obtained some asymptotic and exact representations in Fisher–Snedecor $\mathcal{F}$ fading channels. The effective rate analysis of multiple-input single-output (MISO) systems was presented in i.n.i.d. and independent and identically distributed (i.i.d.) Fisher-Snedecor $\mathcal{F}$ fading channels in [19]. In [20], the ASEP of M-ary quadrature amplitude modulation (MQAM) and M-ary pulse amplitude modulation (MPAM), and the average capacity were derived and evaluated in Fisher-Snedecor $\mathcal{F}$ fading channels. The authors in [21] re-investigated the statistical characterization of the sum of i.n.i.d. Fisher-Snedecor $\mathcal{F}$ RVs and presented a simple approximation by using another single $\mathcal{F}$ RV. After that, the authors in [21] further studied the statistical characterization of the ratio of products of $\mathcal{F}$ distributed random variables in [22] and discussed its applications in physical layer security and full-duplex relaying with co-channel interference.

Although the MRC and SC systems over the Fisher-Snedecor $\mathcal{F}$ fading channels have been investigated in [13], [17], and [21], the authors only considered the i.n.i.d. fading environments and the correlation among different branches were not involved. When the distance between antennas is less than 0.38λ in a diversity system, the received signals could be correlated resulting in a decrease of the diversity gain, where λ is the wavelength of the carrier. To be specific, this signal correlation usually occurs in relatively small size mobile equipment because the space between their diversity branches can be too close to keep the received signals independent. Thus, the correlated analysis of the received signals becomes crucial in the performance evaluation of the diversity received systems. Up to now, the correlated distribution in wireless communication diversity systems has been studied extensively in the open research papers. Nevertheless, most of them only considered either the correlated small-scale fading or the correlated shadowing, such as [8], [23]–[30] and references therein. For correlated multipath and shadowing composite distributions, only a few papers have been involved. Based on a GA shadowing distribution, the correlated K and KG distribution were investigated in [31] and [32], respectively. In [33] and [34], the OP of SC receivers was studied over correlated Weibull-gamma fading channels with identical and non-identical fading conditions, respectively. The authors in [35] studied the performance of Micro- and Macro-diversity receivers in correlated Rician-Gamma fading channels. In [36], the bivariate statistics of a double generalized Gamma distribution was investigated to evaluate the performance of vehicle-to-vehicle (V2V) communications. By using an IG shadowing model, bivariate Rayleigh-IG fading distribution has been proposed

and employed to the dual-branch SC and MRC diversity receivers in [37]. In [38], the authors obtained the statistical properties of bivariate Nakagami-lognormal distribution and discussed the correlation properties under micro- and macro-diversity environments. Recently, [39] proposed a bivariate Rician shadowed fading model in which the shadowing follows a Nakagami-m distribution.

To the best of the authors' knowledge, the correlated (bivariate) Fisher–Snedecor $\mathcal{F}$ composite channel model has not been addressed in the published research work. Motivated by the aforesaid observations, we study a bivariate Fisher–Snedecor $\mathcal{F}$ composite distribution and apply it in the diversity systems and the second-order statistics in this paper. Despite that the probability density function (PDF) of a bivariate Fisher–Snedecor $\mathcal{F}$ distribution has been reported in [40], the mathematical form of the PDF is not suitable for the performance analysis of the wireless communication system. In this paper, we further extend our work in [41] and obtain more significant analysis, so the main contributions of this paper are summarized as follows:

- We derive the novel analytical expressions of the statistical characteristics for bivariate Fisher–Snedecor $\mathcal{F}$ distribution including the joint PDF, the joint cumulative distribution function (CDF), the joint moment generating function (MGF), the joint central moments, and power correlation coefficient.
- Capitalizing on the above statistical expressions, the performance metrics of dual-branch SC and MRC systems are investigated, namely the average signal-to-noise ratio (SNR), Amount of Fading (AoF), the OP, the ABEP/ASEP, and the average channel capacity. In particular, the novel and exact expressions of the ABEP/ASEP of several classical modulation schemes are obtained in the light of the multivariate Fox's H-function by employing the Mellin-Barnes type contour integral. However, in the previous work about correlated fading, most of them only considered the OP [26]–[31], [33], [34], [39] and the ABEP of non-coherent modulation schemes [35], [37] whereas the ASEP of coherent and M-ray modulation schemes had to be calculated by using numerical integration [24], [32] or the Parseval's theorem approach [24]. Moreover, the analysis of the average channel capacity has been rarely involved in [23]–[35], [37] except [36].
- We study the average fade duration (AFD) and the level crossing rate (LCR) of a sampled Fisher-Snedecor $\mathcal{F}$ composited fading envelope, and derive their algebraic expressions by utilizing the univariate CDF and the bivariate CDF of a sampled envelope.
- We derive the asymptotic expressions of the OP and the ABEP/ASEP for dual-branch SC and MRC systems at high SNR regions and discuss the influences of the multipath parameters, the shadowing parameters, and the correlation coefficients on the diversity order and the coding gain.
- We analyze the truncated error and the truncated terms of the CDF expression of the dual-branch SC system. The minimum numbers of the truncated terms are calculated under different communication conditions to ensure the target performance. These results are very well-suited to most algebraic representations including double infinite series sums in this paper.

The remainder of this paper is organized as follows: In Section II, the statistical characteristics of the bivariate Fisher–Snedecor $\mathcal{F}$ composite distribution are investigated. The performance analysis of dual-branch SC and MRC receivers is presented in Section III, and section IV gives the second-order statistics of a sampled composited fading envelope. In Section V, the asymptotic analysis and the truncated error are studied. Numerical and simulation results are shown and discussed in Section VI, and the main conclusions are outlined in Section VII.

II. STATISTICAL CHARACTERISTICS OF BIVARIATE FISHER-SNEDECOR $\mathcal{F}$ DISTRIBUTION

A. JOINT PDF

Let X_i $(i = 1, 2)$ be the channel fading envelopes of Nakagami-m processes, with the joint PDF between X_1 and X_2 given in [42, eq.(126)] as

$$f_{X_1,X_2}(x_1,x_2) = \frac{4m^{m+1}(x_1x_2)^m\rho_N^{-(m-1)/2}}{\Gamma(m)(\sqrt{Y_1Y_2})^{(m+1)}(1-\rho_N)} \times I_{m-1}\left[\frac{2mx_1x_2\sqrt{\rho_N}}{\sqrt{Y_1Y_2}(1-\rho_N)}\right]\exp\left[-\frac{m}{1-\rho_N}\left(\frac{x_1^2}{Y_1}+\frac{x_2^2}{Y_2}\right)\right], \quad (1)$$

where $m \geq 1/2$ is the Nakagami-m fading parameter, ρ_N is the power correlation coefficient between X_1^2 and X_2^2, and Y_i is the mean fading power $\mathrm{Y}_i = \mathbb{E}[X_i^2]$ with $\mathbb{E}[\cdot]$ denoting expectation, $I_{m-1}(x)$ represents the modified Bessel function of the first kind and order (m-1) defined in [43, eq. (9.210/1)], $\Gamma(\cdot)$ denotes the gamma function defined in [43, eq.(8.310.1)].

When multipath fading is superimposed on shadowing, Y_i slowly varies and its root-mean-square (rms) can be considered as one RV following the inverse Nakagami-m distribution in [12]. Based on the revised signal model in [15], we let $\mathrm{Y}_i = w_i^2\Omega_i (i = 1, 2)$, where w_i is a normalized inverse Nakagami-m RV with $\mathbb{E}[w_i] = 1$, $\Omega_i = \mathbb{E}\left[R_i^2\right]$ is the mean power of the composite signal envelope R_i, then the PDF in (1) is conditioned on w_i. To describe an inverse Nakagami-m distribution, we let the parameter $w_i = a_i/r_i$, where r_i follows Nakagami-m distribution, then $a_i = \sqrt{(n_i-1)/n_i}$. Using a standard transformation of RVs, the PDF of the bivariate inverse Nakagami-m distribution can be obtained

as

$$f_{W_1,W_2}(w_1,w_2) = \frac{4(n-1)^{n+1}(w_1w_2)^{-(n+2)}}{\Gamma(n)(1-\rho_G)\rho_G^{(n-1)/2}} \times I_{n-1}\left[\frac{2(n-1)\sqrt{\rho_G}}{w_1w_2(1-\rho_G)}\right]\exp\left[-\frac{(n-1)(w_1^{-2}+w_2^{-2})}{1-\rho_G}\right], \tag{2}$$

where $n > 1$ is the inverse Nakagami-m shaping parameter, ρ_G is the power correlation coefficient between w_1^2 and w_2^2. Note that $n \to 1$ denotes the received signals suffer the heavy shadowing, on the contrary, $n \to \infty$ represents the absence of shadowing.

Based on the total probability theorem, the PDF of the bivariate Fisher–Snedecor $\mathcal{F}$ composite envelope can be obtained by averaging the conditional PDF of the Nakagami-m process over the random variation of the rms signal powers. Consequently, the joint PDF of the bivariate Fisher–Snedecor $\mathcal{F}$ composite distribution is written as

$$f_{R_1,R_2}(r_1,r_2) = \int_0^\infty\int_0^\infty f_{Y_1|W_1,Y_2|W_2}(r_1\,|w_1,\,r_2\,|w_2)f_{W_1,W_2}(w_1,w_2)dw_1dw_2. \tag{3}$$

Based on (1), $f_{Y_1|W_1,Y_2|W_2}(r_1\,|w_1,r_2|\,w_1)$ in (3) can be obtained as

$$f_{R_1|W_1,R_2|W_2}(r_1\,|w_1,\,r_2\,|w_1) = \frac{4m^{m+1}(r_1r_2)^m(w_1w_2)^{-(m+1)}\rho_N^{-(m-1)/2}}{\Gamma(m)(\sqrt{\Omega_1\Omega_2})^{(m+1)}(1-\rho_N)} \times I_{m-1}\left[\frac{2mr_1r_2(w_1w_2)^{-1}\sqrt{\rho_N}}{\sqrt{\Omega_1\Omega_2}(1-\rho_N)}\right] \times \exp\left[-\frac{m}{1-\rho_N}\left(\frac{r_1^2}{w_1^2\Omega_1}+\frac{r_2^2}{w_2^2\Omega_2}\right)\right]. \tag{4}$$

Substituting (4) and (2) in (3), and applying the infinite series representations of the modified Bessel function of the first kind defined in [43, eq.(8.447.1)], and after some mathematical manipulations, the joint PDF of the bivariate Fisher–Snedecor $\mathcal{F}$ composite distribution can be derived as

$$f_{R_1,R_2}(r_1,r_2) = \sum_{k=0}^\infty\sum_{l=0}^\infty \frac{4\rho_N^k\rho_G^l\phi\Gamma(\lambda)(\Xi_1\Xi_2)^{(m+k)}}{k!l!\Gamma(m)\Gamma(n)B(k+m,l+n)} \times \prod_{i=1}^2 \frac{r_i^{2m+2k-1}}{\left(\Xi_i r_i^2+1\right)^\lambda}, \tag{5}$$

where $\Xi_i = m(1-\rho_G)/(n-1)(1-\rho_N)\,\Omega_i$, $\lambda = m+k+n+l$, $\phi = (1-\rho_N)^m(1-\rho_G)^n$, and $B(\cdot,\cdot)$ is the beta function defined in [43, eq.(8.384.1)]. With the help of the Appell function of the fourth kind, $F_4[\cdot]$ defined in [43, eq.(9.180.4)], we can obtain the compact expression of (5) as

$$f_{R_1,R_2}(r_1,r_2) = \frac{4\phi}{B^2(m,n)}\left(\prod_{i=1}^2\frac{\Xi_i^m r_i^{2m-1}}{\left(\Xi_i r_i^2+1\right)^{m+n}}\right) \times F_4\left[m+n,\,m+n;\,m,\,n;\,\rho_N\prod_{i=1}^2\frac{\Xi_i r_i^2}{\Xi_i r_i^2+1},\,\rho_G\prod_{i=1}^2\frac{1}{\Xi_i r_i^2+1}\right]. \tag{6}$$

Note that it can be verified that the marginal distributions with respect to r_1 or r_2 from (5) follow the Fisher–Snedecor $\mathcal{F}$ composite distribution given in [15, eq.(5)]. Furthermore, as $\rho_N = \rho_G = 0$, $F_4[\cdot]$ in (6) equals to unity, the joint PDF in (6) can reduce to

$$f_{R_1,R_2}(r_1,r_2) = \prod_{i=1}^2\left(\frac{2\varphi_i^m r_i^{2m-1}}{\left(1+\varphi_i r_i^2\right)^{m+n}B(m,n)}\right), \tag{7}$$

where $\varphi_i = m/(n-1)\Omega_i$, $i = 1, 2$. It is worth highlighting that there exists no correlation between R_1 and R_2 and they are independent of each other from (7). To the best of the authors' knowledge, the PDF expressions in (5) and (6) have not been reported in the previously published technical literature.

B. JOINT CDF

To obtain a corresponding expression of the joint CDF, by making use of [43, eq.(3.194.1/3)] along with some algebraic manipulations, the joint CDF of R_1 and R_2 can be given by

$$F_{R_1,R_2}(r_1,r_2) = \sum_{k=0}^\infty\sum_{l=0}^\infty \frac{\rho_N^k\rho_G^l\phi\Gamma(\lambda)(\Xi_1\Xi_2)^{(m+k)}}{k!l!\Gamma(m)\Gamma(n)B(k+m,l+n)(m+k)^2} \times \prod_{i=1}^2 r_i^{2m+2k}\,{}_2F_1[\lambda,m+k;1+m+k;-\Xi_i r_i^2], \tag{8}$$

where ${}_2F_1[\cdot,\cdot;\cdot;\cdot]$ is the Gauss hypergeometric function [43, eq. (9.100)].

C. JOINT CENTRAL MOMENTS AND POWER CORRELATION COEFFICIENT

By definition in [24, eq.(12)], the joint central moments of the bivariate Fisher–Snedecor $\mathcal{F}$ composite distribution can be obtained as

$$\mu_{R_1,R_2}(q_1,q_2) = \mathbb{E}[r_1^{q_1}r_2^{q_2}] = \int_0^\infty\int_0^\infty r_1^{q_1}r_2^{q_2}f_{R_1,R_2}(r_1,r_2)dr_1dr_2. \tag{9}$$

Substituting (5) into (9), and employing [43, eq.(3.194.3)] and the identities [43, eq.(9.180.1), (9.182.11) and (9.131.1)], after some mathematical manipulations, we have

$$\begin{aligned}&\mu_{R_1,R_2}(q_1,q_2)\\&=\frac{B(m+\frac{q_1}{2},n-\frac{q_1}{2})_2F_1[-\frac{q_1}{2},-\frac{q_2}{2};m;\rho_N]}{B^2(m,n)(B(m+\frac{q_2}{2},n-\frac{q_2}{2})_2F_1[\frac{q_1}{2},\frac{q_2}{2};n;\rho_G])^{-1}}\\&\quad\times\left((n-1)\Omega_1/m\right)^{\frac{q_1}{2}}\left((n-1)\Omega_2/m\right)^{\frac{q_2}{2}},\end{aligned}\tag{10}$$

where $n > q_1/2$ and $n > q_2/2$. As expected, the above expression can be decomposed into two independent parts as follows

$$\begin{aligned}&\mu_{R_1,R_2}(q_1,q_2)\\&=\mu_{Na}(q_1,q_2)\times\mu_{iNa}(q_1,q_2)\\&=\left(\frac{\Omega_1}{m}\right)^{\frac{q_1}{2}}\left(\frac{\Omega_1}{m}\right)^{\frac{q_1}{2}}\frac{\Gamma(m+\frac{q_1}{2})\Gamma(m+\frac{q_2}{2})}{\Gamma^2(m)}{}_2F_1[-\tfrac{q_1}{2},-\tfrac{q_2}{2};m;\rho_N]\\&\quad\times(n-1)^{\frac{q_1}{2}+\frac{q_2}{2}}\frac{\Gamma(n-\frac{q_1}{2})\Gamma(n-\frac{q_2}{2})}{\Gamma^2(n)}{}_2F_1[\tfrac{q_1}{2},\tfrac{q_2}{2};n;\rho_G],\end{aligned}\tag{11}$$

where $\mu_{Na}(q_1,q_2)$ denotes the joint central moments of the bivariate Nakagami-m distribution which can be obtained as [42, eq.(137)], and $\mu_{iNa}(q_1,q_2)$ denotes the joint central moments of the bivariate inverse Nakagami-m distribution which can be obtained in terms of the same steps as (10). It can be observed from (11) that the received signals over composite fading channels can be taken as the product of two independent RVs, where one is multipath fading RV following Nakagami-m distribution and the other is shadowing RV following inverse Nakagami-m distribution.

By definition in [1, eq.(9.195)], the Fisher–Snedecor $\mathcal{F}$ power correlation coefficient between R_1^2 and R_2^2 can be expressed as

$$\begin{aligned}\rho&\triangleq\frac{\mathrm{cov}(r_1^2,r_2^2)}{\sqrt{\mathrm{var}(r_1^2)}\sqrt{\mathrm{var}(r_2^2)}}\\&=\frac{\mathbb{E}[r_1^2r_2^2]-\mathbb{E}[r_1^2]\mathbb{E}[r_2^2]}{\sqrt{\mathbb{E}[r_1^4]-\mathbb{E}^2[r_1^2]}\sqrt{\mathbb{E}[r_2^4]-\mathbb{E}^2[r_2^2]}},\end{aligned}\tag{12}$$

where $\mathbb{E}(r_i^q)=\frac{B(m+q/2,\mathrm{n}-\mathrm{q}/2)}{B(m,n)(m/(n-1)\Omega_i)^{q/2}}$ was given in [15], $n > q/2, i = 1, 2$.

Then, by using (11) and after some straightforward simplifications, the power correlation coefficient can be written in closed-form as

$$\rho\triangleq\frac{{}_2F_1[-1,-1;m;\rho_N]{}_2F_1[1,1;n;\rho_G]-1}{(m+n-1)[m(n-2)]^{-1}},\tag{13}$$

where $n > 2$.

Based on (13), Fig.1 reveals the relation between the Fisher–Snedecor $\mathcal{F}$ power correlation coefficient (ρ) and the shaping parameters (m and n) and correlation coefficients ($\rho_G$andρ_N) of bivariate Nakagami-m and its inverse distributions. It can be observed from Fig.1 that ρ varies from zero to unity as $\rho_G(\rho_N)$ does, which indicates the system performance degrades gradually with the increase of $\rho_G(\rho_N)$. While for a certain value of $\rho_G(\rho_N)$, ρ increases as n grows from $n = 5$, 20 to 50 when $m = 2.5$, and decreases as m grows from $m = 0.5$, 2.5, 5, 20 to $m = 50$ when $n = 5$. These results demonstrate that the correlation coefficients have a more dominating impact on the decrease of the system performance compared with m and/or n at the light shadowing conditions ($n = 20$ and $n = 50$, including the light composite fading case, $m = 50$ and $n = 50$), and ρ approaches $\rho_G(\rho_N)$. While the increase of m can improve slightly the channel conditions and leads to a decrease of ρ at moderate shadowing cases ($n = 5$), and a similar behavior has been observed in [24]. However, at the heavy shadowing cases ($n = 2.5$, including the heavy composite fading case, $m = 0.5$ and $n = 2.5$), ρ decreases quickly. This may be explained that the heavy shadowing becomes a primary factor in degrading the system performance as well as the effect of ρ gets weak. Furthermore, for the extreme cases, i.e., $\rho_G = \rho_N \to 1$ and $\rho_G = \rho_N \to 0$, $\rho \to 1$ and $\rho \to 0$, respectively, independently of the values of m and n. These cases can also be proved in (13) by using [43, eq.(9.122)] and [43, eq.(9.100)].

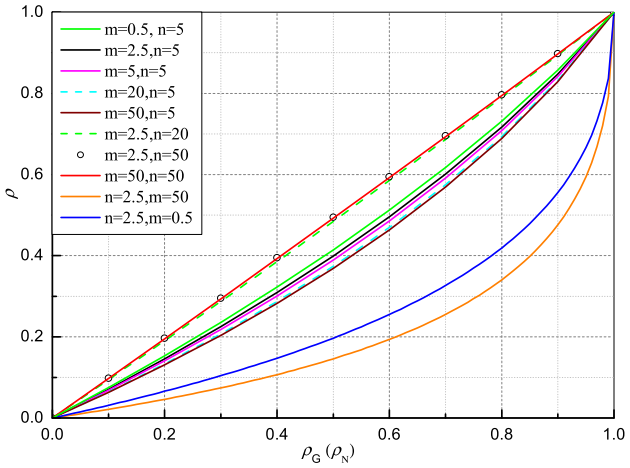

FIGURE 1. The Fisher–Snedecor $\mathcal{F}$ power correlation coefficient ρ as a function of the correlation coefficient ρ_G where $\rho_G = \rho_N$.

D. JOINT MGF

Based on the definition of the joint MGF in [1], the joint MGF of R_1 and R_2 can be given by

$$\begin{aligned}M_{R_1,R_2}(s_1,s_2)&=\mathbb{E}[\exp(-s_1R_1-s_2R_2)]\\&=\int_0^\infty\int_0^\infty\exp(-s_1r_1-s_2r_2)f_{R_1,R_2}(r_1,r_2)dr_1dr_2.\end{aligned}\tag{14}$$

Plugging (5) into (14), and with the help of [44, eq.(07.34.21.0013.01)], after some mathematical manipulations,

the joint MGF of R_1 and R_2 can be obtained as

$$M_{R_1,R_2}(s_1,s_2)=\sum_{k=0}^{\infty}\sum_{l=0}^{\infty}\frac{\rho_N^k\rho_G^l\phi[\Gamma(n)\Gamma(l+n)]^{-1}}{k!l!\pi\Gamma(m)\Gamma(k+m)}\times\prod_{i=1}^{2}G_{3,1}^{1,3}[\frac{4\Xi_i}{s_i^2}|_{m+k}^{1-(n+l),0.5,1}], \quad (15)$$

where $G_{p,q}^{m,n}[\cdot|\cdot]$ denotes the univariate Meijer G-function defined in [44, eq.(07.34.02.0001.01)].

III. DUAL-BRANCH DIVERSITY RECEIVERS

In this section, we consider two classical dual-branch diversity receivers, namely MRC and SC, operating over correlated Fisher–Snedecor $\mathcal{F}$ composite fading channels. For these dual-branch diversity receivers, the equivalent baseband received signal at the ith ($i=1$ and 2) antenna can be given by $r_i=sh_i+n_i$, in which s denotes the complex transmitted symbol with average energy $E_s=\mathbb{E}[|s|^2]$, n_i denotes the complex additive white Gaussian noise (AWGN) with single-sided power spectral density N_0 assumed identical and uncorrelated to two branches, and h_i denotes the complex channel gain with its magnitude $R_i=|h_i|$ following a Fisher–Snedecor $\mathcal{F}$ distribution. Furthermore, the general assumption is made that only the channel fading magnitude has effects on the received signal and the phase can be accurately estimated. Thus, the instantaneous SNR per symbol is expressed as $\gamma_i=R_i^2E_s/N_0$, and its average SNR can be given as $\bar{\gamma}_i=\mathbb{E}\left[R_i^2\right]E_s/N_0=\Omega_iE_s/N_0$.

The PDF of the instantaneous SNR, γ, over the Fisher–Snedecor $\mathcal{F}$ composite fading channels is given by [15]

$$f_\gamma(\gamma)=\frac{\Lambda^m\gamma^{m-1}}{B(m,n)\left(\Lambda\gamma+1\right)^{m+n}}, \quad (16)$$

where $\Lambda=m\big/(n-1)\bar{\gamma}$. The corresponding CDF of the instantaneous SNR is also given by

$$F_\gamma(\gamma)=\frac{(\Lambda\gamma)^m}{mB(m,n)}{}_2F_1[m+n,m;m+1;-\Lambda\gamma]. \quad (17)$$

By using (5) and setting $\gamma_i=r_i^2E_s/N_0$, after a simple variable transformation, the joint PDF of γ_1 and γ_2 over the Fisher–Snedecor $\mathcal{F}$ composite fading channels can be obtained as

$$f_{\gamma_1,\gamma_2}(\gamma_1,\gamma_2)=\sum_{k=0}^{\infty}\sum_{l=0}^{\infty}\frac{\rho_N^k\rho_G^l\phi\Gamma(\lambda)(\eta_1\eta_2)^{m+k}}{k!l!\Gamma(m)\Gamma(n)B(k+m,l+n)}\times\prod_{i=1}^{2}\frac{\gamma_i^{m+k-1}}{(\eta_i\gamma_i+1)^\lambda}, \quad (18)$$

where $\eta_i=m\left(1-\rho_G\right)\big/(n-1)\left(1-\rho_N\right)\bar{\gamma}_i$. Hence, with the aid of [43, eq.(3.194.1)], the corresponding joint CDF of γ_1 and γ_2 can be yielded as

$$F_{\gamma_1,\gamma_2}(\gamma_1,\gamma_2)=\int_0^{\gamma_1}\int_0^{\gamma_2}f_{\gamma_1,\gamma_2}(\gamma_1,\gamma_2)d\gamma_1d\gamma_2=\sum_{k=0}^{\infty}\sum_{l=0}^{\infty}\frac{\rho_G^k\rho_N^l\phi\Gamma(\lambda)(\eta_1\eta_2)^{m+k}(m+k)^{-2}}{k!l!\Gamma(m)\Gamma(n)B(k+m,l+n)}\times\prod_{i=1}^{2}\gamma_i^{m+k}{}_2F_1[\lambda,m+k;1+m+k,-\eta_i\gamma_i]. \quad (19)$$

A. DUAL-BRANCH SC DIVERSITY RECEIVER

1) PDF OF THE OUTPUT SNR AND OUTAGE PROBABILITY

For a dual-branch SC receiver, the instantaneous output SNR can be expressed $\gamma_{SC}=\max(\gamma_1,\gamma_2)$ in [1], and its corresponding CDF is given by $F_{\gamma_{SC}}(\gamma)=F_{\gamma_1,\gamma_2}(\gamma,\gamma)$ in the correlated fading case, where $F_{\gamma_1,\gamma_2}(\gamma,\gamma)$ can be obtained by using (19). As $\rho_N=\rho_G=0$, $F_{\gamma_{SC}}(\gamma)$ can reduce to the i.i.d CDF of two branches in [17, eq.(5)] after some mathematical manipulations.

In order to find the PDF of γ_{SC}, it is readily obtained by taking the first derivative of $F_{\gamma_{SC}}(\gamma)$. However, this can lead to more terms in the expression of the PDF. To this effect, an alternative method in [1, eq.(9.687)] is given by

$$f_{\gamma_{SC}}(\gamma)=\int_0^{\gamma}f_{\gamma_1,\gamma_2}(\gamma,\gamma_2)d\gamma_2+\int_0^{\gamma}f_{\gamma_1,\gamma_2}(\gamma_1,\gamma)d\gamma_1. \quad (20)$$

Substituting (18) in (20), and employing [43, eq.(3.194.1)], after some mathematical manipulations, the PDF of γ_{SC} over correlated Fisher–Snedecor $\mathcal{F}$ composite fading channels can be derived as

$$f_{\gamma_{SC}}(\gamma)=\sum_{k=0}^{\infty}\sum_{l=0}^{\infty}\frac{\rho_N^k\rho_G^l\phi\Gamma(\lambda)(\eta_1\eta_2)^{(m+k)}\gamma^{2(m+k)-1}}{k!l!\Gamma(m)\Gamma(n)B(k+m,l+n)(m+k)}\times\left(\sum_{i=0}^{1}\frac{{}_2F_1[\lambda,m+k;1+m+k;-\eta_{2-i}\gamma]}{(\eta_{i+1}\gamma+1)^\lambda}\right). \quad (21)$$

In general, the OP is defined as the probability that the instantaneous output SNR of SC falls below a given outage threshold γ_{th} in [1]. By utilizing (19), we can obtain the OP of SC receiver by using γ_{th} instead of γ_1 and γ_2 as $P\text{out}=F_{\gamma_1,\gamma_2}(\gamma_{th},\gamma_{th})$.

2) MOMENTS OF THE OUTPUT SNR AND AVERAGE SNR

Based on the definition of the moment in [1], the qth-order moment of γ_{SC} can be expressed as

$$\mu_{\gamma_{SC}}(q)=\mathbb{E}(\gamma_{SC}^q)=\int_0^{\infty}\gamma^qf_{\gamma_{SC}}(\gamma)d\gamma. \quad (22)$$

To solve the integral in (22) after inserting (21) in (22), we use the identities [45, eq.(10) and (17)] to represent $(1+x)^a$ and ${}_2F_1[\cdot,\cdot;\cdot;\cdot]$ in terms of Meijer G-function, and

employ [44, eq.(07.34.21.0011.01)] along with some mathematical manipulations, $\mu_{\gamma_{SC}}(q)$ can be yielded as

$$\mu_{\gamma_{SC}}(q) = \sum_{k=0}^{\infty}\sum_{l=0}^{\infty}\frac{\rho_N^k\rho_G^l\phi[\Gamma(m)\Gamma(n)]^{-1}}{k!l!\Gamma(k+m)\Gamma(l+n)} \times\left(\sum_{i=0}^{1}\eta_{i+1}^{-q}G_{3,3}^{2,3}[\frac{\eta_{2-i}}{\eta_{i+1}}|_{m+k,n+l-q,0}^{1-(n+l),1,1-(m+k+q)}]\right). \quad (23)$$

The average output SNR is an important performance criterion serving as an excellent indicator of the overall system's fidelity. The average output SNR of SC over correlated Fisher–Snedecor $\mathcal{F}$ fading channels can be obtained by setting $q = 1$ in (23), this is, $\bar{\gamma}_{SC} = \mu_{\gamma_{SC}}(1)$.

In addition, the AoF is also considered as a critical performance measure which indicates the severity of fading for the wireless communication system. This measure can be evaluated by using $\mu_{\gamma_{SC}}(q)$. Traditionally, the AoF is defined as

$$AoF = \frac{\mu_{\gamma_{SC}}(2)}{\mu_{\gamma_{SC}}^2(1)} - 1. \quad (24)$$

By setting $q = 1$ and 2 in (23), then inserting them in (24), the expression of AoF over correlated Fisher–Snedecor $\mathcal{F}$ fading channels can be easily obtained. The AoF is typically independent of the average fading power and can be further applied to parameterize the distribution of the SNR of the received signal in the presence of fading, such as the channel quality estimation index (CQEI) presented in [46].

3) MGF OF THE OUTPUT SNR AND ABEP/ASEP

In order to evaluate the ABEP/ASEP of various modulation schemes, the MGF-based approach is usually adopted to simplify the mathematical analysis process. Hence, by using (21) and following the similar procedure as (23) with the aid of [44, eq.(07.34.21.0081.01)], the MGF of γ_{SC} over correlated Fisher–Snedecor $\mathcal{F}$ composite fading can be derived as

$$MGF_{\gamma_{SC}}(s) = \int_0^{\infty}\exp(-s\gamma)f_{\gamma_{SC}}(\gamma)d\gamma = \sum_{k=0}^{\infty}\sum_{l=0}^{\infty}\frac{\rho_N^k\rho_G^l\phi[\Gamma(m)\Gamma(n)]^{-1}}{k!l!\Gamma(k+m)\Gamma(l+n)}\left(\sum_{i=0}^{1}\left(\frac{\eta_{i+1}}{s}\right)^{m+k} \times G_{1,0:1,1:2,2}^{0,1:1,1:1,2}[\frac{\eta_{i+1}}{s},\frac{\eta_{2-i}}{s}|_{-}^{1-(m+k)}|_{0}^{1-\lambda}|_{m+k,0}^{1-(n+l),1}]\right), \quad (25)$$

where $G_{p,q:p_1,q_1:p_2,q_2}^{m,n:m_1,n_1:m_2,n_2}[\cdot|\cdot]$ denotes the bivariate Meijer G-function defined in [47, eq.(13.1)], also named as an extended generalized bivariate Meijer G-function in [48].

By utilizing the MGF expression of γ_{SC} in (25) and the MGF-based approach, the ABEP/ASEP of SC system can be readily obtained for different modulation schemes. For non-coherent binary frequency shift keying (NC-BFSK) and differential binary phase-shift keying (DBPSK), the ABEP of SC system can be expressed as [1]

$$P_e(E) = aMGF_{\gamma_{SC}}(b), \quad (26)$$

where $a = 0.5$, $b = 0.5$ for NC-BFSK, and $a = 0.5$, $b = 1$ for DBPSK. Hence, by using (25), the ABEP of NC-BFSK and DBPSK for SC system over correlated Fisher–Snedecor $\mathcal{F}$ composite fading can be directly yielded as

$$P_e(E) = \sum_{k=0}^{\infty}\sum_{l=0}^{\infty}\frac{a\rho_N^k\rho_G^l\phi[\Gamma(m)\Gamma(n)]^{-1}}{k!l!\Gamma(k+m)\Gamma(l+n)}\left(\sum_{i=0}^{1}\left(\frac{\eta_{i+1}}{b}\right)^{m+k} \times G_{1,0:1,1:2,2}^{0,1:1,1:1,2}[\frac{\eta_{i+1}}{b},\frac{\eta_{2-i}}{b}|_{-}^{1-(m+k)}|_{0}^{1-\lambda}|_{m+k,0}^{1-(n+l),1}]\right). \quad (27)$$

For coherent modulation schemes, such as BPSK, BFSK, and BFSK with minimum correlation, the ABEP at the output of the SC system can be expressed as [1]

$$P_e(E) = \frac{1}{\pi}\int_0^{\pi/2}MGF_{\gamma_{SC}}\left(\frac{g}{\sin^2\theta}\right)d\theta, \quad (28)$$

where g is a constant that depends on the specific modulation schemes. In particular, $g = 1$ for BPSK, and $g = 0.5$ for BFSK, and $g = 0.715$ for BFSK with minimum correlation. In order to find the solution of the integral term in (28), we express the bivariate Meijer G-function in (25) as its alternative definition formula in terms of double Mellin-Barnes type contour integral in [47, eq.(13.1)]. Hence, the exact analytical expression of (28) over correlated Fisher–Snedecor $\mathcal{F}$ composite fading can be derived (see Appendix A for details) as

$$P_e(E) = \sum_{k=0}^{\infty}\sum_{l=0}^{\infty}\frac{\rho_N^k\rho_G^l\phi[\sqrt{\pi}\Gamma(m)\Gamma(n)]^{-1}}{k!l!2\Gamma(k+m)\Gamma(l+n)}\left(\sum_{i=0}^{1}\left(\frac{\eta_{i+1}}{g}\right)^{m+k} \times G_{2,1:1,1:2,2}^{0,2:1,1:1,2}[\frac{\eta_{i+1}}{g},\frac{\eta_{2-i}}{g}|_{m+k}^{1-(m+k),0.5-(m+k)}|_{0}^{1-\lambda}|_{m+k,0}^{1-(n+l),1}]\right). \quad (29)$$

Moreover, the ASEP of MPSK for SC system based on the MGF approach can be given as [1]

$$P_e(E) = \frac{1}{\pi}\int_0^{\pi-\pi/M}MGF_{\gamma_{SC}}\left(\frac{g_{psk}}{\sin^2\theta}\right)d\theta. \quad (30)$$

where $g_{PSK} = \sin^2(\pi/M)$, $M = 2, 4, 8, \ldots$ To solve the integral term in (30), we employ the properties of the sine function and rewrite (30) as

$$P_e(E) = \frac{2}{\pi}\int_0^{\pi/2}MGF_{\gamma_{SC}}\left(\frac{g_{psk}}{\sin^2\theta}\right)d\theta - \frac{1}{\pi}\int_0^{\pi/M}MGF_{\gamma_{SC}}\left(\frac{g_{psk}}{\sin^2\theta}\right)d\theta = I_1 - I_2. \quad (31)$$

For the first integral term I_1 in (31), we can employ the same approach as Appendix A. After some mathematical manipulations, we have

$$I_1 = \sum_{k=0}^{\infty}\sum_{l=0}^{\infty} \frac{\rho_N^k \rho_G^l \phi [\Gamma(m)\Gamma(n)]^{-1}}{k!l!\sqrt{\pi}\Gamma(k+m)\Gamma(l+n)} \left(\sum_{i=0}^{1} \left(\frac{\eta_{i+1}}{g_{psk}} \right)^{m+k} \times G_{2,1:1,1:2,2}^{0,2:1,1:1,2} \left[\frac{\eta_{i+1}}{g_{psk}}, \frac{\eta_{2-i}}{g_{psk}} \middle|_{m+k}^{1-(m+k),0.5-(m+k)} \middle|_{0}^{1-\lambda} \middle|_{m+k,0}^{1-(n+l),1} \right] \right). \tag{32}$$

While for the second integral term I_2 in (31), we consider the similar steps as (29) and use the definition of the multivariable Fox's H-function in terms of double Mellin-Barnes type contour integral in [49, eq.(A.1)]. The detailed derivation procedure of I_2 can be found in Appendix B. Hence, by using the results of I_1 and I_2, the exact analytical expression of (31) over correlated Fisher–Snedecor $\mathcal{F}$ composite fading can be written as (33), shown at the bottom of the next page.

Finally, by using the MGF-based method, the ASEP of MQAM for SC system can be given as [1]

$$P_e(E) = \frac{4c}{\pi}\int_0^{\pi/2} MGF_{\gamma_{SC}}\left(\frac{g_{QAM}}{\sin^2\theta}\right) d\theta - \frac{4c^2}{\pi}\int_0^{\pi/4} MGF_{\gamma_{SC}}\left(\frac{g_{QAM}}{\sin^2\theta}\right) d\theta, \tag{34}$$

where $c = 1 - 1/\sqrt{M}$, and $g_{QAM} = 3/2(M-1)$. Similarly, we adopt the same steps that are used to derive (31), the exact analytical expression of (34) can be obtained as (35), shown at the bottom of the next page.

4) AVERAGE CHANNEL CAPACITY

The channel capacity, in Shannon's sense, is a core performance measure since it provides the maximum achievable transmission rate in which the errors are recoverable. The average channel capacity of the SC can be expressed as

$$\bar{C}_{\gamma_{sc}} = \frac{B}{\ln 2}\int_0^{\infty} \ln(1+\gamma) f_{\gamma_{sc}}(\gamma) d\gamma, \tag{36}$$

where B denotes the bandwidth of the channel. By using (21) and the identity [45, eq.(11)] to represent $\ln(1+x)$ in terms of Meijer G-function, with the help of [44, eq.(07.34.21.0081.01)], the average channel capacity of the SC over correlated Fisher–Snedecor $\mathcal{F}$ composite fading can be obtained as

$$\bar{C}_{\gamma_{sc}} = \sum_{k=0}^{\infty}\sum_{l=0}^{\infty} \frac{B\rho_N^k \rho_G^l \phi [\Gamma(m)\Gamma(n)]^{-1}}{k!l!\ln 2\,\Gamma(k+m)\Gamma(l+n)} \times \left(\sum_{i=0}^{1} G_{1,1:2,1:2,2}^{1,1:1,2:1,2} \left[\frac{1}{\eta_{i+1}}, \frac{\eta_{2-i}}{\eta_{i+1}} \middle|_{n+l}^{1-(m+k)} \middle|_{1,0}^{1,1} \middle|_{m+k,0}^{1-(n+l),1} \right] \right). \tag{37}$$

B. DUAL-BRANCH MRC DIVERSITY RECEIVER

For a dual-branch MRC diversity receiver, the instantaneous output SNR per symbol is expressed as $\gamma_{\text{MRC}} = \gamma_1 + \gamma_2$ in [1]. Under a correlated fading environment, it is difficult to directly find a simple and closed-form expression of the PDF of γ_{MRC}, and the PDF-based performance analysis usually becomes cumbersome and tedious. To this effect, the MGF-based approach is considered to evaluate the OP, the ABEP /ASEP, and the average channel capacity of the dual-branch MRC diversity receiver over correlated Fisher–Snedecor $\mathcal{F}$ composite fading channels.

1) MOMENTS OF THE OUTPUT SNR AND AVERAGE SNR

With the aid of the binomial identity defined in [43, eq.(1.111)], the qth-order moments of $\gamma_{\text{MRC}}\gamma_{MRC}$ can be written as

$$\mu_{\gamma_{MRC}}(q) = \mathbb{E}[\gamma_{MRC}^q] = \mathbb{E}[(\gamma_1+\gamma_2)^q] = \sum_{i=0}^{q}\binom{q}{i}\mathbb{E}[\gamma_1^i \gamma_2^{q-i}]. \tag{38}$$

By using (18) and the similar steps as (10), the corresponding closed-form expression of the qth-order moments of γ_{MRC} over correlated Fisher–Snedecor $\mathcal{F}$ composite fading channels can be derived as

$$\mu_{\gamma_{MRC}}(q) = \sum_{i=0}^{q}\binom{q}{i}\left(\frac{(n-1)\bar{\gamma}_1}{m}\right)^i \left(\frac{(n-1)\bar{\gamma}_2}{m}\right)^{q-i} \times \frac{\Gamma(m+i)\Gamma(m+q-i)\Gamma(n-i)\,{}_2F_1(-i,-q+i;m;\rho_N)}{\Gamma^2(m)\Gamma^2(n)[\Gamma(n-q+i)\,{}_2F_1(-i,-q+i;n;\rho_G)]^{-1}}. \tag{39}$$

By setting $q = 1$ in (39) and using [43, eq. (9.155.4)], and after some straightforward simplifications, the average output SNR of the dual-branch MRC system can be calculated as

$$\bar{\gamma}_{MRC} = \mu_{\gamma_{MRC}}(1) = \bar{\gamma}_1 + \bar{\gamma}_2. \tag{40}$$

Similarly, by setting $q = 1$ and $q = 2$ in (39), the AoF of the dual-branch MRC system can also be obtained.

2) MGF OF THE OUTPUT SNR AND ABEP/ASEP

Based on the definition of MGF and using (18) with the aid of [43, eq.(7.811.5)], the MGF of γ_{MRC} can be expressed as

$$M_{\gamma_{MRC}}(s) = M_{\gamma_1,\gamma_2}(s,s) = \mathbb{E}[\exp(-s(\gamma_1+\gamma_2))] = \sum_{k=0}^{\infty}\sum_{l=0}^{\infty} \frac{\rho_N^k \rho_G^l \phi [\Gamma(k+m)]^{-1}}{k!l!\Gamma(m)\Gamma(n)\Gamma(l+n)} \times \prod_{i=1}^{2} G_{1,2}^{2,1}\left[\frac{s}{\eta_i}\middle|_{0,n+l}^{1-m-k}\right]. \tag{41}$$

By using (26) and (41), the ABEP expression of NC-BFSK and BDPSK for the dual-branch MRC system over correlated Fisher–Snedecor $\mathcal{F}$ composite fading channels can be written

as

$$P_e(E) = \sum_{k=0}^{\infty}\sum_{l=0}^{\infty} \frac{a\rho_N^k \rho_G^l \phi[\Gamma(k+m)]^{-1}}{k!l!\Gamma(m)\Gamma(n)\Gamma(l+n)} \times \prod_{i=1}^{2} G_{1,2}^{2,1}[\frac{b}{\eta_i}|_{0,n+l}^{1-m-k}]. \quad (42)$$

Similar to (29), by employing the definition of the bivariate Meijer G-function in [47], the ABEP of BPSK, BFSK, and BFSK with minimum correlation at the output of MRC system can be expressed as

$$P_e(E) = \sum_{k=0}^{\infty}\sum_{l=0}^{\infty} \frac{\rho_N^k \rho_G^l \phi[\Gamma(m)\Gamma(n)]^{-1}}{k!l!2\sqrt{\pi}\Gamma(k+m)\Gamma(l+n)} \times G_{1,1:2,1:2,1}^{0,1:1,2:1,2}[\frac{\eta_1}{g}, \frac{\eta_2}{g}|_{0}^{0.5}|_{m+k}^{1,1-n-l}|_{m+k}^{1,1-n-l}]. \quad (43)$$

For the MPSK modulation scheme, the exact analytical expression of ASEP for the dual-branch MRC system over Fisher–Snedecor $\mathcal{F}$ composite fading can be obtained as (44), shown at the bottom of the next page by utilizing the same steps as (33). Similarly, the exact analytical expression of ASEP of MQAM for the dual-branch MRC system can also be yielded as (45), shown at the bottom of the next page.

3) OUTAGE PROBABILITY

By utilizing the MGF-based approach, the OP of the dual-branch MRC system is given by [1]

$$P_{out}(\gamma_{th}) = \Pr(\gamma_{MRC} < \gamma_{th}) = F_{\gamma_{MRC}}(\gamma_{th}) = L^{-1}\left[\frac{MGF_{\gamma_{MRC}}(s)}{s}; \gamma_{MRC}\right]\Big|_{\gamma_{MRC}=\gamma_{th}}, \quad (46)$$

where $F_{\gamma_{MRC}}(\cdot)$ denotes the CDF of γ_{MRC}, and $\mathrm{L}^{-1}[\cdot;\cdot]$ represents the inverse Laplace transform. In order to solve the inverse Laplace transform in (46), the CDF of γ_{MRC} can be expressed as

$$F_{\gamma_{MRC}}(\gamma) = \frac{1}{2\pi j}\int_{\mathbb{C}} \exp(s\gamma) M_{\gamma_{MRC}}(s)/s ds. \quad (47)$$

where $j = \sqrt{-1}$ and C denotes the appropriate contour. By substituting (41) in (47), and based on the definition of the univariate Meijer G-function in [44], after some mathematical manipulations, the exact analytical expression of the CDF of γ_{MRC} over correlated Fisher–Snedecor $\mathcal{F}$ composite fading channels can be obtained (see Appendix C for details) as

$$F_{\gamma_{MRC}}(\gamma) = \sum_{k=0}^{\infty}\sum_{l=0}^{\infty} \frac{\rho_N^k \rho_G^l \phi[\Gamma(m)\Gamma(n)]^{-1}}{k!l!\Gamma(k+m)\Gamma(l+n)} \times G_{1,0:1,2:1,2}^{0,0:2,1:2,1}[1/\eta_1\gamma, 1/\eta_2\gamma|_{-}^{1}|_{0,n+l}^{1-m-k}|_{0,n+l}^{1-m-k}]. \quad (48)$$

Hence, the OP of the dual-branch MRC system can be calculated after replacing γ with γ_{th} based on the above expression. In addition, the OP in (46) can be also calculated by applying the Euler summation based algorithm for the inversion of CDFs in [1, Appendix 9B.1]. In what follows, the upper and lower bounds of the OP for the dual-branch MRC system are considered as [1]

$$F_{\gamma_{\max}}\left(\frac{\gamma_{th}}{2}\right) \le P_{out}(\gamma_{th}) \le F_{\gamma_{\min}}\left(\frac{\gamma_{th}}{2}\right), \quad (49)$$

where $\gamma_{\max} = \max(\gamma_1, \gamma_2)$, $\gamma_{\min} = \min(\gamma_1, \gamma_2)$, $F_{\gamma_{\max}}(\cdot)$ and $F_{\gamma_{\min}}(\cdot)$ denote the corresponding CDF of $\gamma_{\max}$ and $\gamma_{\min}$, and can be expressed, respectively, as

$$F_{\gamma_{\max}}(\gamma) = \Pr\{\gamma_1 < \gamma, \gamma_2 < \gamma\} = F_{\gamma_1,\gamma_2}(\gamma,\gamma). \quad (50\text{-a})$$

$$F_{\gamma_{\min}}(\gamma) = 1 - \Pr\{\gamma_1 > \gamma, \gamma_2 > \gamma\} = F_{\gamma_1}(\gamma) + F_{\gamma_2}(\gamma) - F_{\gamma_1,\gamma_2}(\gamma,\gamma). \quad (50\text{-b})$$

On the basis of (17) and (19), the above two expressions can be readily obtained, respectively.

4) AVERAGE CHANNEL CAPACITY

According to the MGF-based approach in [50], the average channel capacity of the dual-branch MRC system can be given as

$$\bar{C}_{\gamma_{MRC}} = \frac{B}{\ln 2}\int_0^{\infty} \mathrm{Ei}(-s)\left[\frac{\partial}{\partial s} M_{\gamma_{MRC}}(s)\right] ds, \quad (51)$$

where $\mathrm{Ei}(\cdot)$ is the exponential integral function defined in [43, eq.(8.221.1)]. By employing (41) and with the help of

$$P_e(E) = \sum_{k=0}^{\infty}\sum_{l=0}^{\infty} \frac{\rho_N^k \rho_G^l \phi[\Gamma(n)\Gamma(l+n)]^{-1}}{k!l!\sqrt{\pi}\Gamma(m)\Gamma(k+m)} \left(\sum_{i=0}^{1}\left(\frac{\eta_{i+1}}{g_{psk}}\right)^{m+k}\left(G_{2,1:1,1:2,2}^{0,2:1,1:1,2}[\frac{\eta_{i+1}}{g_{psk}}, \frac{\eta_{2-i}}{g_{psk}}|_{m+k}^{1-(m+k),0.5-(m+k)}|_{0}^{1-\lambda}|_{m+k,0}^{1-(n+l),1}] - \frac{z^{m+k+0.5}}{2\pi} H_{2,1:1,1:2,2:1,1}^{0,2:1,1:1,2:1,1}[\frac{z\eta_{i+1}}{g_{psk}}, \frac{z\eta_{2-i}}{g_{psk}}, -z|_{(-0.5-m-k:1,1,1)}^{(0.5-m-k:1,1,1),(1-m-k:1,1,0)}|_{(0:1)}^{(1-\lambda:1)}|_{(m+k:1),(0:1)}^{(1-n-l:1),(1:1)}|_{(0:1)}^{(0.5:1)}]\right)\right). \quad (33)$$

$$P_e(E) = \sum_{k=0}^{\infty}\sum_{l=0}^{\infty} \frac{2c\rho_N^k \rho_G^l \phi[\Gamma(m)\Gamma(n)]^{-1}}{k!l!\sqrt{\pi}\Gamma(k+m)\Gamma(l+n)} \left(\sum_{i=0}^{1}\left(\frac{\eta_{i+1}}{g_{QAM}}\right)^{m+k}\left(G_{2,1:1,1:2,2}^{0,2:1,1:1,2}[\frac{\eta_{i+1}}{g_{QAM}}, \frac{\eta_{2-i}}{g_{QAM}}|_{m+k}^{1-(m+k),0.5-(m+k)}|_{0}^{1-\lambda}|_{m+k,0}^{1-(n+l),1}] - \frac{0.5^{m+k+0.5}c}{\pi} H_{2,1:1,1:2,2:1,1}^{0,2:1,1:1,2:1,1}[\frac{\eta_{i+1}}{2g_{QAM}}, \frac{\eta_{2-i}}{2g_{QAM}}, -0.5|_{(-0.5-m-k:1,1,1)}^{(0.5-m-k:1,1,1),(1-m-k:1,1,0)}|_{(0:1)}^{(1-\lambda:1)}|_{(m+k:1),(0:1)}^{(1-n-l:1),(1:1)}|_{(0:1)}^{(0.5:1)}]\right). \quad (35)$$

[44, eq.(07.34.20.0002.01)], the first-order derivative of the MGF of γ_{MRC} with respect to s in (51) can be deduced as

$$\begin{aligned}&\frac{\partial}{\partial s}M_{\gamma_{MRC}}(s)\\&=\sum_{k=0}^{\infty}\sum_{l=0}^{\infty}\frac{\rho_N^k\rho_G^l\phi[\Gamma(n)\Gamma(l+n)]^{-1}}{k!l!\Gamma(m)\Gamma(k+m)}\\&\quad\times\left(\sum_{i=0}^{1}\frac{-1}{\eta_{i+1}}G_{1,2}^{2,1}[\frac{s}{\eta_{i+1}}|_{0,-1+n+l}^{-m-k}]G_{1,2}^{2,1}[\frac{s}{\eta_{2-i}}|_{0,n+l}^{1-m-k}]\right).\end{aligned}\tag{52}$$

Here, we represent Ei $(-s)$ in terms of Meijer G-function as

$$\mathrm{Ei}(-s)=-G_{1,2}^{2,0}[s|_{0,0}^{1}].\tag{53}$$

Then, by plugging (52) and (53) into (51), and employing [44, eq.(07.34.21.0011.01)] along with some mathematical manipulations, the exact analytical expression of the average channel capacity for the dual-branch MRC system over correlated Fisher–Snedecor $\mathcal{F}$ composite fading channels can be obtained as

$$\begin{aligned}&\bar{C}_{\gamma_{MRC}}\\&=\sum_{k=0}^{\infty}\sum_{l=0}^{\infty}\frac{B\rho_N^k\rho_G^l\phi[\Gamma(n)\Gamma(l+n)]^{-1}}{\ln 2k!l!\Gamma(m)\Gamma(k+m)}\\&\quad\times\left(\sum_{i=0}^{1}G_{2,1:1,2:1,2}^{1,2:2,0:2,1}[\eta_{i+1},\frac{\eta_{i+1}}{\eta_{2-i}}|_{m+k}^{0,1-(n+l)}|_{0,0}^{1}|_{0,(n+l)}^{1-(m+k)}]\right).\end{aligned}\tag{54}$$

IV. LEVEL CROSSING RATE AND AVERAGE FADE DURATION

The LCR and AFD are two important examples to characterize higher-order statistics of the received signal envelope in small-scale multipath and/or large-scale shadowing fading environments. They are very helpful to design and select error control techniques and diversity systems since they can provide useful information about the burst error statistics. The former denotes the expected rate at which the fading envelope crosses a specified threshold level in a positive (or negative) direction, whereas the latter is defined as the average period of time in which the envelope stays below this specified threshold level. Traditionally, the joint PDF of the continuous fading envelope and its time derivative has been employed to calculate them based on Rice's method [51]. In [52], the authors proposed an alternative analytical approach in which the LCR and the AFD of a sampled random process can be obtained according to the univariate CDF and the bivariate CDF of a sampled envelope. Recently this approach has been used to evaluate the LCR and the AFD of a sampled Rician shadowed fading envelope in [39]. In [52], the LCR of a sampled random process is expressed as

$$LCR(\mu)=\frac{\Pr\{R_1<\mu,R_2>\mu\}}{T_s},\tag{55}$$

where $R_1\triangleq R(t)$ and $R_2R\triangleq(t+Ts)$ are correlated and identically distributed random variables, $R(t)$ is the continuous-time envelope, μ is a specified threshold level and Ts denotes the sampling period. Moreover, the marginal CDF of R_1 and R_2 can be given as $F_R(x)\triangleq F_{R_1}(x)\triangleq F_{R_2}(x)$. Therefore, the compact form of the LCR can be expressed by using the marginal CDF of R_1 and the bivariate CDF of R_1 and R_2 in [52] as follows

$$LCR(\mu)=\frac{F_{R_1}(\mu)-F_{R_1,R_2}(\mu,\mu)}{T_s},\tag{56}$$

where $F_{R_1}(\mu)$ can be found in [15, eq.(11)]. By substituting (8) into (56), the LCR can be obtained as

$$\begin{aligned}LCR(\mu)&=\frac{(\Lambda_1\mu^2)^m}{T_smB(m,n)}{}_2F_1[m+n,m;m+1;-\Lambda_1\mu^2]\\&\quad-\sum_{k=0}^{\infty}\sum_{l=0}^{\infty}\frac{\rho_N^k\rho_G^l\phi\Gamma(\lambda)(\Xi_1\Xi_2)^{(m+k)}(m+k)^{-2}}{k!l!T_s\Gamma(m)\Gamma(n)B(k+m,l+n)}\\&\quad\times\prod_{i=1}^{2}\mu^{2m+2k}{}_2F_1[\lambda,m+k;1+m+k,-\Xi_i\mu^2].\end{aligned}\tag{57}$$

where $\Lambda_1=m/(n-1)\Omega_1$. Based on the definition of the AFD in [52], the AFD of a sampled random process can be written as

$$AFD(\mu)=\frac{\Pr(R_1<\mu)}{LCR(\mu)}=\frac{T_sF_{R_1}(\mu)}{F_{R_1}(\mu)-F_{R_1,R_2}(\mu,\mu)}.\tag{58}$$

Similar to (57), (58) can also be readily calculated.

$$\begin{aligned}P_e(E)&=\sum_{k=0}^{\infty}\sum_{l=0}^{\infty}\frac{\rho_N^k\rho_G^l\phi[\Gamma(n)\Gamma(l+n)]^{-1}}{k!l!\sqrt{\pi}\Gamma(m)\Gamma(k+m)}\left(G_{1,1:2,1:2,1}^{0,1:1,2:1,2}[\frac{\eta_1}{g_{psk}},\frac{\eta_2}{g_{psk}}|_0^{0.5}|_{m+k}^{1,1-n-l}|_{m+k}^{1,1-n-l}]\right.\\&\quad\left.-\frac{z^{0.5}}{2\pi}H_{1,1:2,1:2,1:1,1}^{0,1:1,2:1,2:1,1}[\frac{z\eta_1}{g_{psk}},\frac{z\eta_2}{g_{psk}},-z|_{(-0.5:1,1,1)}^{(0.5:1,1,1)}|_{(m+k:1)}^{(1:1),(1-n-l:1)}|_{(m+k:1)}^{(1:1),(1-n-l:1)}|_{(0:1)}^{(0.5:1)}]\right).\end{aligned}\tag{44}$$

$$\begin{aligned}P_e(E)&=\sum_{k=0}^{\infty}\sum_{l=0}^{\infty}\frac{2c\rho_N^k\rho_G^l\phi[\Gamma(n)\Gamma(l+n)]^{-1}}{k!l!\sqrt{\pi}\Gamma(m)\Gamma(k+m)}\left(G_{1,1:2,1:2,1}^{0,1:1,2:1,2}[\frac{\eta_1}{g_{QAM}},\frac{\eta_2}{g_{QAM}}|_0^{0.5}|_{m+k}^{1,1-n-l}|_{m+k}^{1,1-n-l}]\right.\\&\quad\left.-\frac{c}{\sqrt{2}\pi}H_{1,1:2,1:2,1:1,1}^{0,1:1,2:1,2:1,1}[\frac{\eta_1}{2g_{QAM}},\frac{\eta_2}{2g_{QAM}},-0.5|_{(-0.5:1,1,1)}^{(0.5:1,1,1)}|_{(m+k:1)}^{(1:1),(1-n-l:1)}|_{(m+k:1)}^{(1:1),(1-n-l:1)}|_{(0:1)}^{(0.5:1)}]\right).\end{aligned}\tag{45}$$

V. ASYMPTOTIC ANALYSIS AND TRUNCATION ERROR

In this section, the asymptotic behavior of the aforementioned performance expressions will be discussed, such as the OP and the ABEP expressions for dual-branch SC and MRC system. Then we investigate the rate of convergence of the infinite series sum by employing the truncation error analysis and give some calculation results by taking the CDF expression of the output SNR for the dual-branch SC system as an instance.

A. ASYMPTOTIC ANALYSIS

For the sake of obtaining more insights on how the channel parameters and the correlation coefficients affect the diversity order and the coding gain, the asymptotic performance analysis at high SNR regions is especially useful for wireless diversity communication systems. The diversity order refers to the slope of the OP or ABEP (ASEP) curve versus the average SNR in a log-log scale. In general, the larger the slope of the curve, and the higher the diversity order. While the coding gain is considered as the shifting degree of OP or ABEP (ASEP) line to the left versus SNR in a log-log scale. Thus, at high average SNR regions, the asymptotic OP or ABEP (ASEP) can be expressed as [53]

$$P_x \approx (G_c \cdot \bar{\gamma})^{-G_d}, \tag{59}$$

where G_c is the coding gain and G_d is the diversity order, P_x denotes the OP or the ABEP (ASEP). In what follows, we derive the high SNR asymptotic performance expressions of SC and MRC system over correlated Fisher–Snedecor $\mathcal{F}$ composite fading, by taking the OP and the ABEP of DPSK as examples, and point out their diversity orders.

1) DUAL-BRANCH SC RECEIVER

When the average SNR $\bar{\gamma}_i \to \infty$, by using the series representation of a hypergeometric function in [43, eq.(9.100)], the PDF of the output SNR for SC system in (21) can be approximated as

$$f_{\gamma_{SC}}(\gamma) \approx \sum_{k=0}^{\infty}\sum_{l=0}^{\infty} \frac{2\rho_N^k \rho_G^l \phi \Gamma^2(\lambda)(\eta_1\eta_2)^{(m+k)}\gamma^{2(m+k)-1}}{k!l!\Gamma(m)\Gamma(n)\Gamma(k+m+1)\Gamma(l+n)}. \tag{60}$$

By using (60), the asymptotic CDF and MGF of the output SNR for SC system can be deduced, respectively, as

$$F_{\gamma_{SC}}(\gamma) \approx \sum_{k=0}^{\infty}\sum_{l=0}^{\infty} \frac{\rho_N^k \rho_G^l \phi \Gamma^2(\lambda)(\eta_1\eta_2)^{(m+k)}[\Gamma(m)\Gamma(n)]^{-1}}{k!l!\Gamma(k+m+1)\Gamma(l+n)(m+k)}\gamma^{2(m+k)}. \tag{61-a}$$

$$MGF_{\gamma_{SC}}(s) \approx \sum_{k=0}^{\infty}\sum_{l=0}^{\infty} \frac{2\rho_N^k \rho_G^l \phi \Gamma^2(\lambda)(\eta_1\eta_2)^{(m+k)}\Gamma(2m+2k)}{k!l!\Gamma(m)\Gamma(n)\Gamma(k+m+1)\Gamma(l+n)}s^{-2(m+k)}. \tag{61-b}$$

Therefore, the asymptotic expressions of the OP and the ABEP of DPSK for SC system can be deduced, respectively, as

$$P_{out}(\gamma_{th}) \approx \sum_{k=0}^{\infty}\sum_{l=0}^{\infty} \frac{\rho_N^k \rho_G^l \phi \Gamma^2(\lambda)(\eta_1\eta_2)^{(m+k)}[\Gamma(m)\Gamma(n)]^{-1}}{k!l!\Gamma(k+m+1)\Gamma(l+n)(m+k)}\gamma_{th}^{2(m+k)}. \tag{62-a}$$

$$P_e(E) \approx \sum_{k=0}^{\infty}\sum_{l=0}^{\infty} \frac{2a\rho_N^k \rho_G^l \phi \Gamma^2(\lambda)(\eta_1\eta_2)^{(m+k)}\Gamma(2m+2k)}{k!l!\Gamma(m)\Gamma(n)\Gamma(k+m+1)\Gamma(l+n)b^{2(m+k)}}. \tag{62-b}$$

Finally, in order to observe the diversity order of the OP, (62-a) needs to be further approximated and is written as the form of (59). As $\bar{\gamma}_1 = \bar{\gamma}_2 = \bar{\gamma} \to \infty$, (62-a) can be further simplified, (the mathematical derivation is provided in Appendix D), as

$$P_{out}(\gamma_{th}) \approx \left(\left(\frac{\phi_2 F_1(m+n, m+n; n; \rho_G)}{m^2 B^2(m,n)(\Psi\gamma_{th})^{-2m}}\right)^{-\frac{1}{2m}} \cdot \bar{\gamma}\right)^{-2m}. \tag{63-a}$$

where $\Psi = m(1-\rho_G)/(n-1)(1-\rho_N)$. By using a similar method in (63-a), the asymptotic expression of the ABEP of DPSK can be further simplified as

$$P_e(E) \approx \left(\left(\frac{2a\phi\Gamma(2m)F_1(m+n, m+n; n; \rho_G)}{mB^2(m,n)(b/\Psi)^{2m}}\right)^{-\frac{1}{2m}} \cdot \bar{\gamma}\right)^{-2m}. \tag{63-b}$$

Based on the definition in (59), it is evident from (63-a) and (63-b) that their diversity order G_d is $2m$ regardless of the larger-scale parameters and the correlation coefficients.

2) DUAL-BRANCH MRC RECEIVER

Since the diversity order and the code gain can be observed by using the asymptotic value of the MGF function when $s \to \infty$ [3], with the aid of the asymptotic formula of the univariate Meijer G-function defined in [44, eq.(07.34.06.0018.01)], the MGF of the output SNR for MRC system in (41) can be approximated as

$$MGF_{\gamma_{MRC}}(s) \approx \sum_{k=0}^{\infty}\sum_{l=0}^{\infty} \frac{\rho_N^k \rho_G^l \phi \Gamma(k+m)\Gamma^2(\lambda)(\eta_1\eta_2)^{m+k}}{k!l!\Gamma(m)\Gamma(n)\Gamma(l+n)s^{2(m+k)}}. \tag{64}$$

By using (47), we perform the inverse Laplace transform to the above expression, the asymptotic CDF of the output SNR for MRC system can be obtained as

$$F_{\gamma_{MRC}}(\gamma) \approx \sum_{k=0}^{\infty}\sum_{l=0}^{\infty} \frac{\rho_N^k \rho_G^l \phi \Gamma(k+m)\Gamma^2(\lambda)(\eta_1\eta_2\gamma^2)^{m+k}}{k!l!\Gamma(m)\Gamma(n)\Gamma(l+n)\Gamma(2m+2k+1)}. \tag{65}$$

Then, the asymptotic expressions of the OP and the ABEP of DPSK for MRC system can be deduced, respectively, as

$$P_{out}(\gamma_{th}) \approx \sum_{k=0}^{\infty}\sum_{l=0}^{\infty} \frac{\rho_N^k \rho_G^l \phi \Gamma(k+m)\Gamma^2(\lambda)(\eta_1\eta_2\gamma_{th}^2)^{m+k}}{k!l!\Gamma(m)\Gamma(n)\Gamma(l+n)\Gamma(2m+2k+1)}. \tag{66-a}$$

$$P_e(E) \approx \sum_{k=0}^{\infty}\sum_{l=0}^{\infty} \frac{a\rho_N^k \rho_G^l \phi \Gamma(k+m)\Gamma^2(\lambda)(\eta_1\eta_2)^{m+k}}{k!l!\Gamma(m)\Gamma(n)\Gamma(l+n)b^{2(m+k)}}. \tag{66-b}$$

Therefore, similar to the mathematical derivation of Appendix D, as $\bar{\gamma}_1 = \bar{\gamma}_2 = \bar{\gamma} \to \infty$, (66-a) and (66-b) can be further simplified, respectively, as

$$P_{out}(\gamma_{th}) \approx \left(\left(\frac{\phi\Gamma^2(m+n)\,{}_2F_1(m+n, m+n; n; \rho_G)}{\Gamma^2(n)\Gamma(2m+1)\,(\Psi\gamma_{th})^{-2m}} \right)^{-\frac{1}{2m}} \cdot \bar{\gamma} \right)^{-2m}. \tag{67-a}$$

$$P_e(E) \approx \left(\left(\frac{a\phi\Gamma^2(m+n)\,{}_2F_1(m+n, m+n; n; \rho_G)}{\Gamma^2(n)\,(b/\Psi)^{2m}} \right)^{-\frac{1}{2m}} \cdot \bar{\gamma} \right)^{-2m}. \tag{67-b}$$

In terms of the definition in (59), it can be seen from (67-a) and (67-b) that their diversity order G_d is $2m$. Furthermore, as $\rho_N = \rho_G = 0$, (67-a) can reduce to the i.i.d case as [13, eq.(10)] when L=2.

From the aforesaid asymptotic analysis, as expected, the dual-branch SC and MRC systems have identical diversity orders over correlated Fisher–Snedecor $\mathcal{F}$ composite fading, and only the small-scale fading parameters have heavy impacts on the diversity order, while other parameters, namely the larger-scale parameters and the correlation coefficients, have impacts only on the coding gain. Moreover, the aforementioned asymptotic expressions not only have a convenient and simply algebraic form that is helpful in the numerical analysis but also can reveal some insights for wireless communication system design.

B. TRUNCATION ERROR

In the aforesaid sections, most algebraic formulas include double infinite series sums, and their rates of convergence need to be investigated for exact target performance. Hence, we considered the CDF expression of the output SNR for the dual-branch SC system in (19) as an example to discuss the truncated error and the truncated terms. It is noted that these results are also suitable for the other expressions in this paper.

We assume that K and L are the numbers of truncated terms, and expand the expression of (19) as

$$F_{\gamma_1,\gamma_2}(\gamma,\gamma) = \left(\frac{\phi(\eta_1\eta_2\gamma^2)^m}{\Gamma(m)\Gamma(n)} \right)(Z_0 + Z_1 + Z_2), \tag{68}$$

where

$$Z_0 = \sum_{k=0}^{K} \frac{\rho_N^k(\eta_1\eta_2\gamma^2)^k}{k!\Gamma(k+m)(m+k)^2} \left(\sum_{l=0}^{L} \frac{\rho_G^l\Gamma^2(\lambda)}{l!\Gamma(l+n)} \times {}_2F_1[\lambda, m+k; 1+m+k, -\eta_1\gamma]\,{}_2F_1[\lambda, m+k; 1+m+k, -\eta_2\gamma] \right), \tag{69-a}$$

$$Z_1 = \sum_{k=0}^{K} \frac{\rho_N^k(\eta_1\eta_2\gamma^2)^k}{k!\Gamma(k+m)(m+k)^2} \left(\sum_{l=L+1}^{K_1} \frac{\rho_G^l\Gamma^2(\lambda)}{l!\Gamma(l+n)} \times {}_2F_1[\lambda, m+k; 1+m+k, -\eta_1\gamma]\,{}_2F_1[\lambda, m+k; 1+m+k, -\eta_2\gamma] \right), \tag{69-b}$$

$$Z_2 = \sum_{k=K+1}^{K_1} \frac{\rho_N^k(\eta_1\eta_2\gamma^2)^k}{k!\Gamma(k+m)(m+k)^2} \left(\sum_{l=0}^{K_1} \frac{\rho_G^l\Gamma^2(\lambda)}{l!\Gamma(l+n)} \times {}_2F_1[\lambda, m+k; 1+m+k, -\eta_1\gamma]\,{}_2F_1[\lambda, m+k; 1+m+k, -\eta_2\gamma] \right), \tag{69-c}$$

$K_1 \to \infty$. Hence, the truncated error after truncating the double infinite series in (68) can be obtained as

$$E_T = \left(\frac{\phi(\eta_1\eta_2\gamma^2)^m}{\Gamma(m)\Gamma(n)} \right)(Z_1 + Z_2). \tag{70}$$

With the aid of Mathematica software package, we adopt the numerical analysis method to calculate K (L) at a given target accuracy. To meet the given target accuracy, it is a key factor to choose the values of K (L) and K_1 in (69-a) and (69-b). Without loss of generality, we assume $K = L$. To obtain the minimum value of K (L), we need to adjust it until E_T in (70) is less than the given target accuracy. In fact, the target accuracy can be achieved as long as K_1 is greater than K. For example, $K_1 = K + 50$ is enough for all of the cases in this paper when the truncated error satisfies $E_T < 2.0 \times 10^{-6}$. Based on the above method, we obtain the minimum number of truncated terms, K (L), required in (19) at a given error accuracy ($E_T < 2.0 \times 10^{-6}$). In Table 1-4, the minimum values of K (L) have been summarized for different normalized SNR ($\gamma/\bar{\gamma}$), m, n and $\rho_N(\rho_G)$, respectively. It can be observed that the number of truncated terms grows rapidly with the increase of the value of the shadowing parameter or/and the correlation coefficients while it changes slightly as the normalized SNR or/and the multipath parameter increases. Interestingly, ρ_G has more impacts on the number of truncated terms than ρ_N in Table 4.

VI. NUMERICAL RESULTS AND DISCUSSION

Capitalizing on the previous derived analytical expressions, we will present various numerical and simulation results under different correlated Fisher–Snedecor $\mathcal{F}$ fading and shadowing scenarios in this section. In simulations,

TABLE 1. Minimum number of terms, $K(L)$, required in (19) at $E_T < 2.0 \times 10^{-6}$ for different normalized SNR $\gamma/\bar{\gamma}$ ($m = 2$, $n = 5$, $\rho_G = \rho_N = 0.5$).

Normalized SNR	0dB	4dB	8dB	12dB	16dB	20dB
$K(L)$	29	30	30	30	30	31

TABLE 2. Minimum number of terms, $K(L)$, required in (19) at $E_T < 2.0 \times 10^{-6}$ for different m ($n = 5$, $\rho_G = \rho_N = 0.5$, $\gamma/\bar{\gamma} = 5$dB).

m	0.5	1	2	2.5	4	5
$K(L)$	29	30	30	30	30	31

TABLE 3. Minimum number of terms, $K(L)$, required in (19) at $E_T < 2.0 \times 10^{-6}$ for different n ($m = 2$, $\rho_G = \rho_N = 0.5$, $\gamma/\bar{\gamma} = 5$dB).

n	1.5	5	15	25	40	50
$K(L)$	22	30	51	68	92	107

TABLE 4. Minimum number of terms, $K(L)$, required in (19) at $E_T < 2.0 \times 10^{-6}$ for different $\rho_N(\rho_G)$ ($m = 2$, $n = 5$, $\gamma/\bar{\gamma} = 5$dB).

ρ_N	ρ_G	$K(L)$	ρ_N	ρ_G	$K(L)$
0.2	0.2	11	0.5	0.8	101
	0.5	30	0.8	0.2	55
	0.8	100		0.5	56
0.5	0.2	18		0.8	100
	0.5	30	0.9	0.9	215

we adopted the simulation approach described in [54] to first generate two groups of correlated distributed Nakagami-m variables, and then apply their ratios to obtain the correlated Fisher–Snedecor $\mathcal{F}$ variables. The simulations that are obtained via generating no less than 10^6 iterations are compared with the analytical results. Simulation results match well with the numerical analysis and confirm the accuracy of our derivations. In simulation and numerical analysis, several different combinations of the multipath parameters, the shadowing parameters, and the correlation coefficients are considered to discuss their respective impacts on the performance of dual-branch SC and MRC systems. Furthermore, for the aforementioned bivariate Meijer G-function and triple-variable Fox's H-function in this paper, a Mathematica implementation was provided in [48], a Python code has been introduced in [55], a GPU-enabled MATLAB routine was developed in [56]. They can be applied to evaluate these special functions. Unfortunately, some expressions including these special functions become difficult to converge $\gamma_{\text{th}} = 0$dB when the truncated terms get larger. For example, $K(L) = 215$ as $\rho_N = \rho_G = 0.9$ shown in Table 4. However, these cases have less influence on our conclusions in this paper.

By using (23), in Fig.2, we show the first branch normalized average output SNR ($\bar{\gamma}_{SC}/\bar{\gamma}_1$) of SC as a function of the multipath fading parameter (m) for various wireless communication scenarios over correlated Fisher–Snedecor $\mathcal{F}$ fading channels. It can be seen from Fig.2 that the average SNR gain

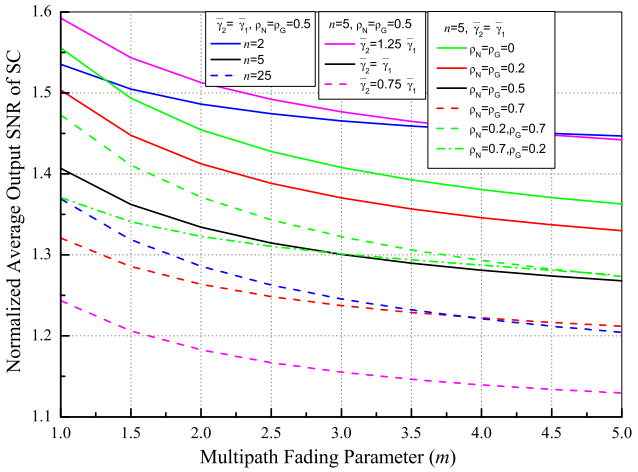

FIGURE 2. First-branch normalized average output SNR ($\bar{\gamma}_{SC}/\bar{\gamma}_1$) of dual-branch SC as a function of the multipath fading parameter (m) over correlated Fisher–Snedecor $\mathcal{F}$ fading channels.

decreases gradually as m grows for all scenarios. Especially for the smaller values of m, this gain degrades quite rapidly. For different shadowing parameters ($n = 2$, 5, and 25) when $\rho_G = \rho_N = 0.5$ and $\bar{\gamma}_1 = \bar{\gamma}_2$, it is interesting to note that the average SNR gain decreases from the heavy shadowing ($n = 2$), the moderate shadowing ($n = 5$) to the light shadowing ($n = 25$). These results show that the SC system would like to choose one branch with the maximum SNR and hold it when the channel conditions get better (m and/or n increase) and two branches have high SNR. Likewise, the average SNR gain also degrades as only the correlation coefficients (ρ_G and/or ρ_N) increase with the fixed values of other parameters. It may be explained that the increase of the correlation coefficients leads to the worse received signals, and the average output SNR of the SC system tends to that of a single branch (i.e., without diversity). In particular, for the uncorrelated case ($\rho_G = \rho_N = 0$), the average SNR gain reaches its maximum limit. Whereas for the unequal correlation coefficient cases, namely $\rho_N = 0.2$, $\rho_G = 0.7$ and $\rho_N = 0.7$, $\rho_G = 0.2$, the average SNR gain of the former is higher than that of the latter for the lower values of m, which indicates the small-scale correlation coefficient (ρ_N) shows a larger influence on the system performance than the shadowing correlation coefficient (ρ_G) at the high fading severity. As expected, for the unbalanced average SNR per branch, the case of $\bar{\gamma}_2 = 1.25\bar{\gamma}_1$ obtains a larger SNR gain than the case of $\bar{\gamma}_2 = 0.75\bar{\gamma}_1$.

On the basis of (24), Fig.3 illustrates the AoF of dual-branch SC system as a function of the multipath fading parameter (m) for various channel conditions over correlated Fisher–Snedecor $\mathcal{F}$ fading channels. As expected, it is observed that the values of the AoF show similar behaviors as the average SNR gain in Fig.2 as m and/or n increases. On the contrary, the AoF increases with the increase of the correlation coefficients ($\rho_G = \rho_N = 0, 0.2, 0.5, 0.7$). This is because the system performance degrades when the correlation coefficients get larger. Whereas for the unequal

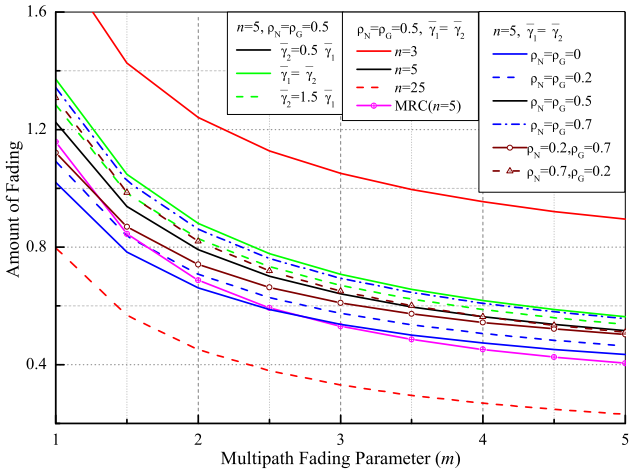

FIGURE 3. AoF of dual-branch SC system as a function of the multipath fading parameter (m) over correlated Fisher–Snedecor $\mathcal{F}$ fading channels.

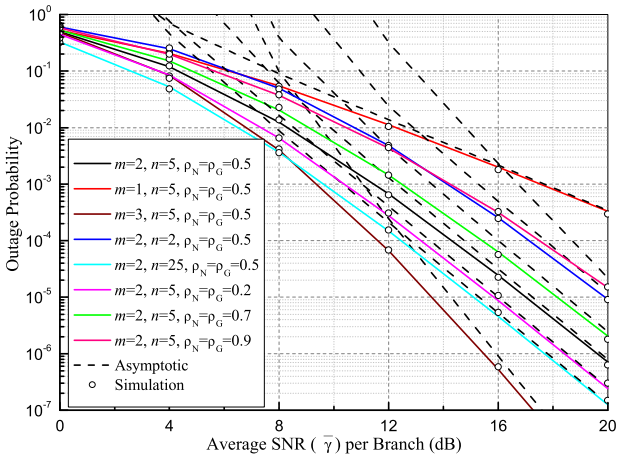

FIGURE 4. Outage Probability of dual-branch SC system as a function of the average SNR with $\gamma_{\text{th}} = 0$dB over correlated $\mathcal{F}$ composite fading channels.

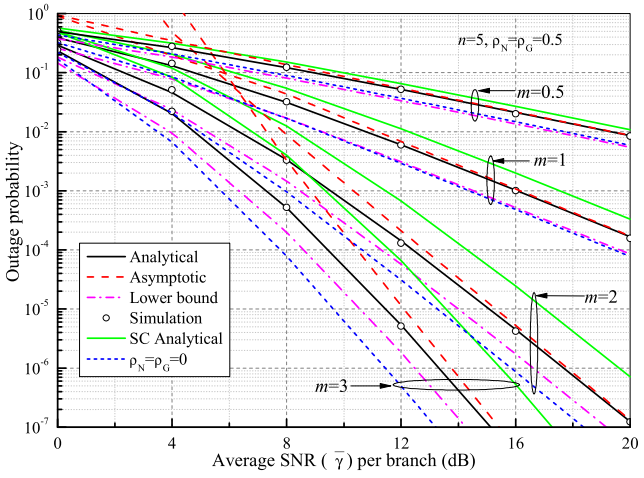

FIGURE 5. Outage Probability of dual-branch MRC system as a function of the average SNR with $\gamma_{\text{th}} = 0$dB over correlated $\mathcal{F}$ composite fading channels.

correlation coefficient cases, namely $\rho_N = 0.2, \rho_G = 0.7$ and $\rho_N = 0.7, \rho_G = 0.2$, the AoF value of the former is smaller than that of the latter for the lower values of m, and a similar result has been obtained in Fig.2. In addition, the AoF value of the unequal SNR cases ($\bar{\gamma}_2 = 1.25\bar{\gamma}_1$ and $\bar{\gamma}_2 = 0.75\bar{\gamma}_1$) is higher than the one of the equal SNR case ($\bar{\gamma}_1 = \bar{\gamma}_2$), and this indicates the latter can improve the system performance. For comparison purposes, the AoF of the dual-branch MRC system is also presented. It is evident that the AoF of MRC has a lower value than that of SC, and the MRC system can provide better system performance. It is due to the fact that the output SNR of the MRC system is the sum of the average SNR of two branches, while that of the SC system is the maximum one. Furthermore, it can be seen from Fig.3 that the maximum value and the minimum value of AoF occur as $n = 3$ and $n = 25$. This result shows that the shadowing parameter causes more effect on the AoF by comparing them with the correlation coefficients and the unequal SNR.

By using (19), the outage probability of dual-branch SC receiver is plotted in Fig. 4 as a function of the average output SNR ($\bar{\gamma}$) per branch with the outage threshold $\gamma_{th} = 0dB$ over correlated $\mathcal{F}$ composite fading channels. As anticipated, the OP gets better as m ($m = 1, 2, 3$) and/or n ($n = 2, 5, 25$) increases, and/or as the correlation coefficients ($\rho_G = \rho_N = 0.9, 0.7, 0.5, 0.2$) reduce when a moderate scenario ($m = 2$, $n = 5$, $\rho_G = \rho_N = 0.5$) is assumed as a benchmark. In particular, the small-scale fading parameter (m) has an important impact on the slope of the OP performance, namely, the larger the value of m, the larger the curve slope. On the other hand, the shadowing parameter and the correlation coefficients have an impact on the coding gain of the OP performance in the high SNR region, as shown in (63-a). Whereas the increase of the shadowing parameter leads to a larger coding gain than the decrease of the correlation coefficients. Likewise, by using (48), Fig.5 depicts the OP of dual-branch MRC receiver as a function of the average output SNR ($\bar{\gamma}$) per branch with the outage threshold $\gamma_{th} = 0dB$, $n = 5$ and $\rho_G = \rho_N = 0.5$. It can be seen from Fig.5 that the OP significantly improves with the increase of m. As expected, the OP of MRC outperforms that of SC, and the uncorrelated case ($\rho_G = \rho_N = 0$) provides the best system performance under all considered communication scenarios. However, the lower bound of the OP of the MRC receiver remains relatively loose in whole SNR regimes regardless of the value of m. In addition, the asymptotic results are also presented in Fig.4 and Fig.5. We can observe that the asymptotic results keep tight with the exact results at high average SNR values. Interestingly, it is noted that the asymptotic results can rapidly converge to the exact results with the smaller values of m and/or the correlated level, and/or the larger value of n.

Based on (27), Fig.6 plots the ABEP of DPSK for dual-branch SC receiver as a function of the average SNR per bit in the same communication scenarios as those used in Fig.4. In Fig.6, the exact analytical results, the asymptotic results,

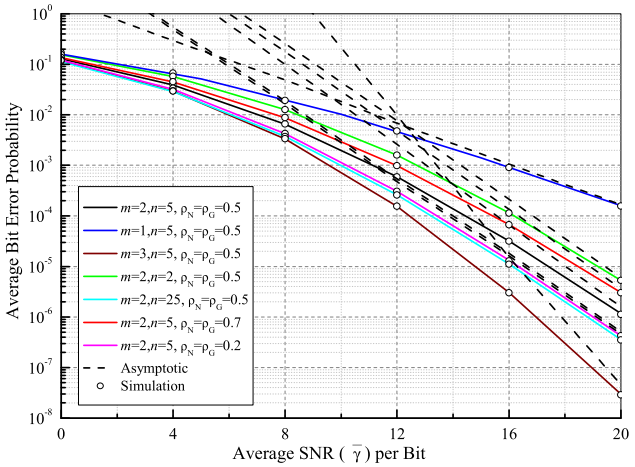

FIGURE 6. Average BEP of DPSK of dual-branch SC system as a function of the average SNR over correlated $\mathcal{F}$ composite fading channels.

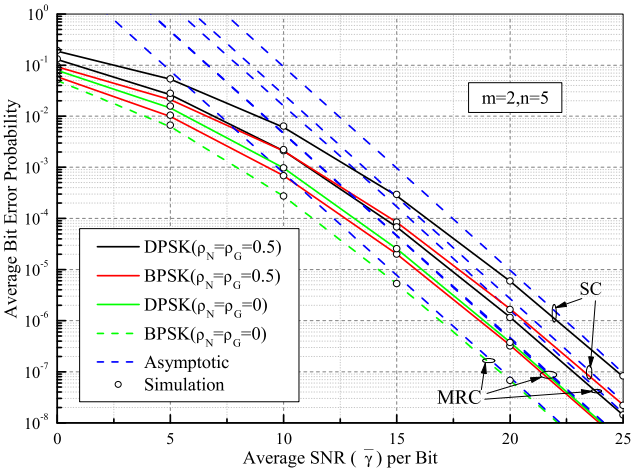

FIGURE 7. Average BEP of BPSK and BDPSK of dual-branch SC and MRC systems as a function of the average SNR over correlated $\mathcal{F}$ composite fading channels.

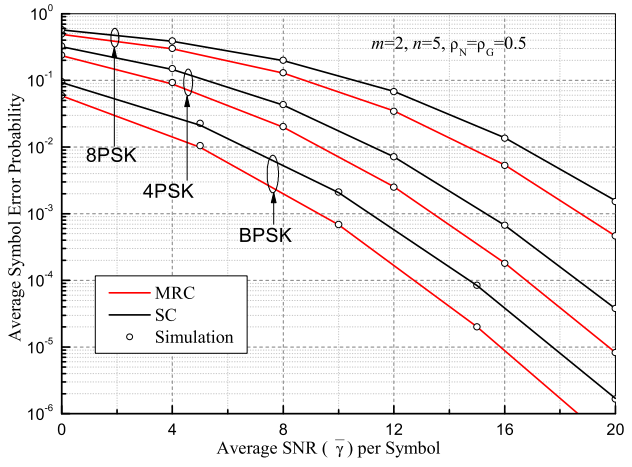

FIGURE 8. Average SEP of MPSK of dual-branch SC and MRC systems as a function of the average SNR over correlated $\mathcal{F}$ composite fading channels.

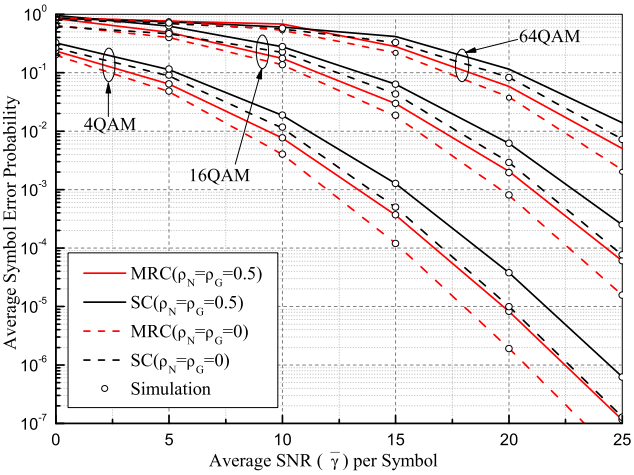

FIGURE 9. Average SEP of MQAM of dual-branch SC and MRC systems as a function of the average SNR over correlated $\mathcal{F}$ composite fading channels.

and the simulations are presented, respectively. As expected, we can obtain the same conclusions as those in Fig.4 from these results. In Fig.7, we demonstrate the ABEP performance of BPSK and DPSK for dual-branch SC and MRC receivers as a function of the average SNR per bit in a moderate fading and shadowing scenario ($m = 2$ and $n = 5$). For comparison purposes, it is observed from Fig.7 that the ABEP of MRC receiver outperforms that of SC receiver, and the ABEP of BPSK is better than that of DPSK because the differential modulation can result in more performance loss than the coherent one. Moreover, the uncorrelated case ($\rho_G = \rho_N = 0$) shows the best system performance.

Furthermore, Fig.8 and Fig.9 plot the ASEP of MPSK and MQAM for dual-branch SC and MRC as a function of the average SNR per symbol in the case of $m = 2$, $n = 5$ and $\rho_G = \rho_N = 0.5$. It is clear that the ASEP performance of SC and MRC diversity systems improves as the average SNR per symbol grows, and degrades because the distances among the symbols get smaller with the increase of the value of M.

On the basis of (37) and (54), the average capacity per unit bandwidth of SC and MRC receiver versus the first branch average SNR is plotted in Fig.10 for several different communication conditions. From Fig.10 (a) to Fig.10 (d), it is evident that the average capacity improves with the increase of the value of m, n and/or $\bar{\gamma}_1$, respectively. However, the increase of the correlation coefficients leads to the reduction of the average capacity. For the unequal average SNR case, the larger the value of $\bar{\gamma}_2$, the larger the average capacity. This is because the SC system is apt to choose the second branch as its output. On the other hand, the increasing trends of average capacity become slight when the value of m and/or n becomes larger, and/or when the value of the correlation coefficient becomes smaller. These results suggest these parameters have no dominating impact on the average capacity. Moreover,

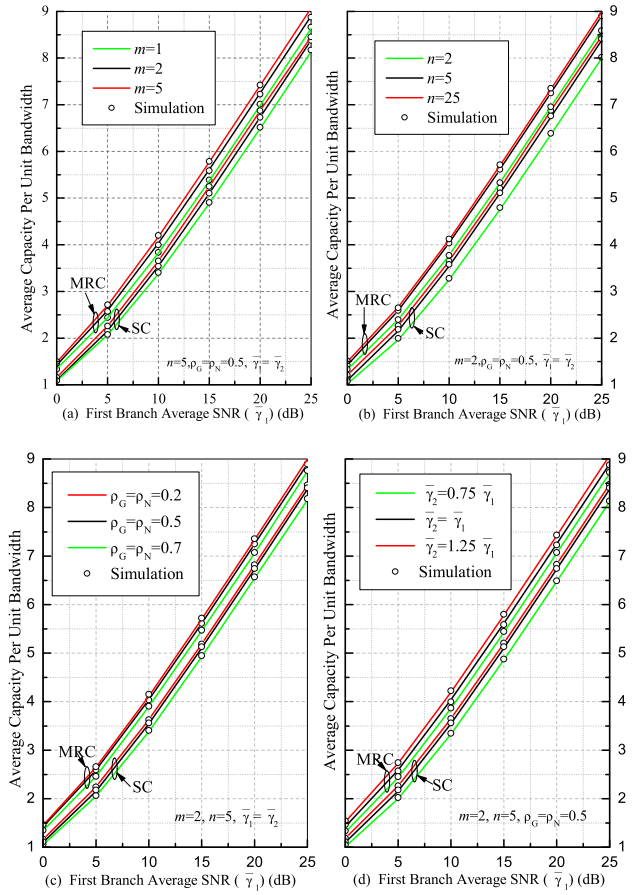

FIGURE 10. Average capacity per unit bandwidth of SC and MRC receivers versus the first branch average SNR over correlated $\mathcal{F}$ composite fading channels.

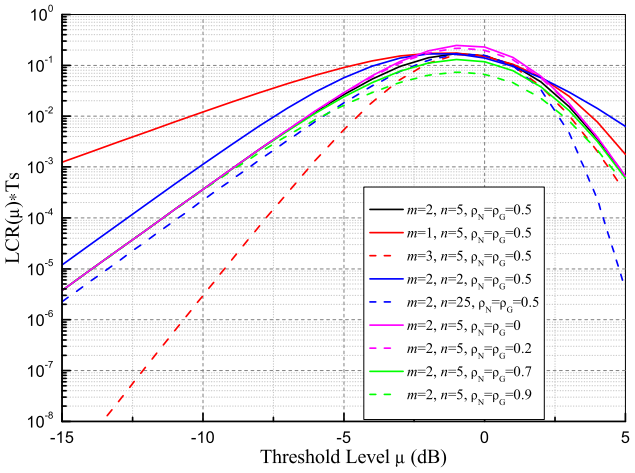

FIGURE 11. LCR·Ts of a sampled correlated $\mathcal{F}$ composite fading envelope as a function of the specified level μ with $\Omega_i = 1$ $(i = 1, 2)$.

the average capacity of dual-branch MRC is higher than that of the dual-branch SC receiver in all cases.

Finally, Fig.11 illustrates the LCR·Ts as a function of the specified lever μ with $\Omega_i = 1(i = 1, 2)$ for several different communication scenarios as those used in Fig.4. As it was expected, when the other parameters are fixed, the LCR decreases obviously with the increase of the value of m. This demonstrates that the fades take place less frequently when the fading severity reduces (i.e., m increases). Moreover, the shape of LCR gets narrower and falls fast on both sides as the value of m grows, which may be explained by the fact that m characterizes the fast fading of the instantaneous signal envelope. On the contrary, the correlation coefficients show less effect on the LCR at lower threshold levels whereas the LCR decreases slightly as the correlation coefficients grow at higher threshold levels. The former can be corroborated since the first term without the correlation coefficients in (57) plays a more important role in the final results than the second term, and the latter is because two successive sampling values of the envelope tend to be identical and result in the second term larger with the increase of the correlation coefficients. As compared to the correlation parameters, the shadowing parameters constitute a more significant impact on the LCR across all the threshold levels. However, it is interesting to note that the LCR decreases quickly as the shadowing varies from heavy ($n = 2$) to light ($n = 25$) at higher threshold levels. This is because the shadowing parameter depicts the slow fading of the instantaneous signal envelope and has more influence on the power mean value of the signal envelope. In Fig.12, we plot the ADF/Ts versus the specified lever μ with $\Omega_i = 1(i = 1, 2)$ under these same scenarios as Fig.11. Since LCR and AFD are inversely proportional, some similar conclusions can be also obtained. It is interesting that these curves show a floor effect at lower threshold levels. This is due to the fact that the least value of a fading duration is Ts (one sampling period), this is to say, the value of ADF/Ts tends to 1.

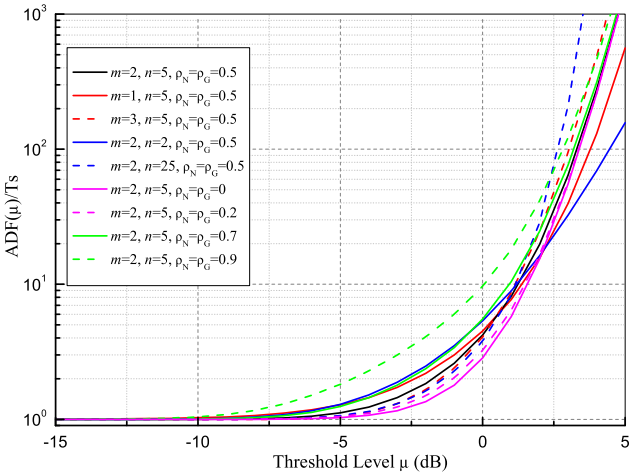

FIGURE 12. ADF/Ts of a sampled correlated $\mathcal{F}$ composite fading envelope as a function of the specified level μ with $\Omega_i = 1$ $(i = 1, 2)$.

VII. CONCLUSION

In this paper, we investigated a bivariate Fisher–Snedecor $\mathcal{F}$ composite distribution with identical shaping parameters. The novel theoretical representations including the joint PDF, the joint CDF, and the joint moments for this distribution

were derived. Based on these theoretical results, we analyzed the performance of dual-branch SC and MRC receivers over correlated Fisher–Snedecor $\mathcal{F}$ composite fading channels and evaluated the LCR and the AFD of a sampled Fisher-Snedecor $\mathcal{F}$ composited fading envelope. Simulation results matched well with the numerical analysis and confirmed the validity of the theoretical expressions under various correlated fading and shadowing scenarios.

APPENDIX A

Let $x = sin^2\theta$ and $dx = 2sin\theta cos\theta d\theta$, then by inserting (25) in (28), and after some necessary changes of variables, (28) can be written as

$$P_e(E) = \sum_{k=0}^{\infty}\sum_{l=0}^{\infty}\frac{\rho_N^k\rho_G^l\phi[\Gamma(m)\Gamma(n)]^{-1}}{k!l!2\pi\Gamma(k+m)\Gamma(l+n)} \times\left(\sum_{i=0}^{1}\left(\frac{\eta_{i+1}}{g}\right)^{m+k}\int_0^1 x^{m+k-0.5}(1-x)^{-0.5}\Upsilon_1 dx\right), \tag{A-1}$$

where $\Upsilon_1 = G_{1,0:1,1:2,2}^{0,1:1,1:1,2}[\frac{x\eta_{i+1}}{g}, \frac{x\eta_{2-i}}{g}|_{-}^{1-(m+k)}|_{0}^{1-\lambda}|_{m+k,0}^{1-(n+l),1}]$.

Based on the alternative definition of the bivariate Meijer G-function in [47, eq.(13.1)], Υ_1 can be expanded as

$$\Upsilon_1 = \left(\frac{1}{2\pi j}\right)^2\int_{\mathbb{C}_1}\int_{\mathbb{C}_2}\frac{\Gamma(m+k+t_1+t_2)\Gamma(t_2)}{\Gamma(1+t_2)[\Gamma(n+l+t_2)]^{-1}} \times\frac{\Gamma(\lambda+t_1)\Gamma(-t_1)}{[\Gamma(m+k-t_2)]^{-1}}\left(\frac{x\eta_{i+1}}{g}\right)^{t_1}\left(\frac{x\eta_{2-i}}{g}\right)^{t_2}dt_1dt_2, \tag{A-2}$$

where $j = \sqrt{-1}$ and $\mathbb{C}_i$ denotes the ith appropriate contour which starts at the point $\tau_i - j\infty$ and goes to the point $\tau_i - j\infty$ with τ_i is a constant value, $i \in \{1, 2\}$.

Therefore, the integral term with respect to x in (A-1) with the aid of [43, eq.(3.191.3)] can be obtained as

$$\Upsilon_2 = \int_0^1 x^{m+k+t_1+t_2-0.5}(1-x)^{-0.5}dx = \frac{\sqrt{\pi}\Gamma(m+k+0.5+t_1+t_2)}{\Gamma(m+k+1+t_1+t_2)}. \tag{A-3}$$

By using (A-1) and (A-2), and the alternative definition of the bivariate Meijer G-function, after some mathematical manipulations, (29) can be obtained.

APPENDIX B

Let $x = sin^2\theta$, $dx = 2sin\theta cos\theta d\theta$, then by inserting (25) in I_2, and after some necessary changes of variables, I_2 can be written as

$$I_2 = \sum_{k=0}^{\infty}\sum_{l=0}^{\infty}\frac{\rho_N^k\rho_G^l\phi[\Gamma(n)\Gamma(l+n)]^{-1}}{k!l!2\pi\Gamma(m)\Gamma(k+m)}\left(\sum_{i=0}^{1}\left(\frac{\eta_{i+1}}{g_{psk}}\right)^{m+k}\cdot I_3\right) \tag{B-1}$$

where $I_3 = \int_0^z x^{m+k-0.5}(1-x)^{-0.5}\Upsilon_3 dx$, z $= \sin^2(\pi/\mathrm{M})z = sin^2(\pi/M)$, Υ_3 can be obtained by replacing g in (A-2) with g_{PSK}. Therefore, the integral term with respect to x in I_3 with the aid of [43, eq.(8.391)] can be obtained as

$$\Upsilon_4 = \int_0^z x^{m+k+t_1+t_2-0.5}(1-x)^{-0.5}dx = \mathrm{B}_z(m+k+t_1+t_2+0.5, 0.5), \tag{B-2}$$

where $B_x(\cdot,\cdot)$ is the incomplete beta function defined in [43, eq.(8.391)]. To obtain the solution of the integral term I_3 in (B-1), we use the identity [57, eq.(06.19.26.0010.01)] to represent $B_x(\cdot,\cdot)$ in (B-2) in terms of the definition of Meijer G-function. To this end, Υ_4 can be yielded as

$$\Upsilon_4 = \frac{z^{m+k+t_1+t_2+0.5}}{\sqrt{\pi}}\frac{1}{2\pi j}\int_{\mathbb{C}_3}\frac{\Gamma(0.5+m+k+t_1+t_2+t_3)}{\Gamma(1.5+m+k+t_1+t_2+t_3)} \times\Gamma(0.5+t_3)\Gamma(-t_3)(-z)^{t_3}dt_3. \tag{B-3}$$

We combine Υ_3 and Υ_4 into I_3, and use the definition of the multivariable Fox's H-function in terms of multiple Mellin–Barnes type contour integral defined in [49], and after some mathematical manipulations, I_3 can be re-expressed as

$$I_3 = \frac{z^{m+k+0.5}}{\sqrt{\pi}}H_{2,1:1,1:2,2:1,1}^{0,2:1,1:1,2:1,1}[\frac{z\eta_{i+1}}{g_{psk}}, \frac{z\eta_{2-i}}{g_{psk}}, -z |_{(-0.5-m-k:1,1,1)}^{(0.5-m-k:1,1,1),(1-m-k:1,1,0)}|_{(0:1)}^{(1-\lambda:1)}|_{(m+k:1),(0:1)}^{(1-n-l:1),(1:1)}|_{(0:1)}^{(0.5:1)}], \tag{B-4}$$

where $\mathrm{H}_{\mathrm{p,q;p_1,q_1:\cdots:p_3,q_3}}^{\mathrm{m,n:m_1,n_1:\cdots:m_3,n_3}}[\cdot|\cdot]$ denotes a triple-variable Fox's H-function defined in [49]. By substituting (B-4) into (B-1), the analytical expression of (36) can be obtained.

APPENDIX C

Based on the definition of the univariate Meijer G-function in [44], (41) can be expanded as

$$M_{\gamma_{MRC}}(s) = \sum_{k=0}^{\infty}\sum_{l=0}^{\infty}\frac{\rho_N^k\rho_G^l\phi[\Gamma(n)\Gamma(l+n)]^{-1}}{k!l!\Gamma(m)\Gamma(k+m)} \times\left(\frac{1}{2\pi j}\right)^2\int_{\mathbb{C}_1}\int_{\mathbb{C}_2}\prod_{i=1}^{2}\left(\frac{s}{\eta_i}\right)^{t_i}\Gamma(-t_i) \times\Gamma(n+l-t_i)\Gamma(m+k+t_i)dt_1dt_2. \tag{C-1}$$

By substituting (C-1) in (47), and after some mathematical manipulations, (47) can be rewritten as

$$F_{\gamma_{MRC}}(\gamma) = \sum_{k=0}^{\infty}\sum_{l=0}^{\infty}\frac{\rho_N^k\rho_G^l\phi[\Gamma(n)\Gamma(l+n)]^{-1}}{k!l!\Gamma(m)\Gamma(k+m)} \times\left(\frac{1}{2\pi j}\right)^2\int_{\mathbb{C}_1}\int_{\mathbb{C}_2}(\Upsilon_5)\prod_{i=1}^{2}(\eta_i)^{-t_i} \times\Gamma(m+k+t_i)\Gamma(n+l-t_i)\Gamma(-t_i)dt_1dt_2 \tag{C-2}$$

where $\Upsilon_5 = \frac{1}{2\pi j}\int_{\mathbb{C}_3}s^{(t_1+t_2)-1}\exp(s\gamma)ds$.

Let $s = jx$ in Υ_5, and by using [43, eq.(8.315.2)], Υ_5 can be calculated as

$$\Upsilon_5 = \frac{\gamma^{-t_1-t_2}}{\Gamma(1-t_1-t_2)}. \tag{C-3}$$

By inserting (C-3) in (C-2), and using the definition of the univariate Meijer G-function again, after some algebraic manipulations, (48) can be obtained.

APPENDIX D

By using the definition of the Gauss hypergeometric function [43, eq. (9.100)], (62-a) can be rewritten as

$$P_{out}(\gamma_{th}) \approx \frac{\phi\gamma_{th}^{2m}(\eta_1\eta_2)^m}{mB^2(m,n)} \sum_{k=0}^{\infty} \frac{(m+n)_k(m+n)_k}{k!(m+1)_k(m+k)} \times \left(\rho_N\eta_1\eta_2\gamma_{th}^2\right)^k {}_2F_1(m+n+k, m+n+k; n; \rho_G). \quad \text{(D-1)}$$

where $(x)_p$ is the Pochhammer's symbol defined in [43, p.xliii], $(x)_p = \Gamma(x+p)\big/\Gamma(x)$, with $p \in \mathbb{N}$. As $\bar{\gamma}_i \to \infty$, we ignore the higher-order terms of $\bar{\gamma}_i$ $(k \geq 1)$, the above expression can be further approximated as

$$P_{out}(\gamma_{th}) \approx \frac{\phi\gamma_{th}^{2m}(\eta_1\eta_2)^m}{m^2B^2(m,n)} {}_2F_1(m+n, m+n; n; \rho_G). \quad \text{(D-2)}$$

As $\bar{\gamma}_1 = \bar{\gamma}_2 = \bar{\gamma}$, (D-2) can be simplified as

$$P_{out}(\gamma_{th}) \approx \frac{\phi\, {}_2F_1(m+n, m+n; n; \rho_G)(\Psi\gamma_{th})^{2m}}{m^2B^2(m,n)\bar{\gamma}^{2m}}, \quad \text{(D-3)}$$

where $\Psi = m(1-\rho_G)\big/(n-1)(1-\rho_N)$. Based on the form of (59), (D-3) can be rewritten as (63-a).

REFERENCES

[1] M. K. Simon and M.-S. Alouini, *Digital Communication Over Fading Channels*, 2nd ed. Hoboken, NJ, USA: Wiley, 2005.

[2] Y. J. Chun, S. L. Cotton, H. S. Dhillon, F. J. Lopez-Martinez, J. F. Paris, and S. K. Yoo, "A comprehensive analysis of 5G heterogeneous cellular systems operating over κ–μ shadowed fading channels," *IEEE Trans. Wireless Commun.*, vol. 16, no. 11, pp. 6995–7010, Nov. 2017.

[3] W. Cheng and Y. Huang, "On the performance of adaptive SC/MRC cooperative systems over composite fading channels," *Chin. J. Electron.*, vol. 25, no. 3, pp. 533–540, May 2016.

[4] P. Ramirez-Espinosa and F. J. Lopez-Martinez, "On the utility of the inverse gamma distribution in modeling composite fading channels," in *Proc. IEEE Global Commun. Conf. (GLOBECOM)*, Waikoloa, HI, USA, Dec. 2019, pp. 1–6.

[5] M. Bhatt and S. K. Soni, "A unified performance analysis of energy detector over α-η-μ/Lognormal and α-κ-μ/Lognormal composite fading channels with diversity and cooperative spectrum sensing," *AEÜ-Int. J. Electron. Commun.*, vol. 94, pp. 367–376, Sep. 2018.

[6] Karmeshu and R. Agrawal, "On efficacy of Rayleigh-inverse Gaussian distribution over K-distribution for wireless fading channels," *Wireless Commun. Mobile Comput.*, vol. 7, no. 1, pp. 1–7, Jan. 2007. [Online]. Available: https://dl.acm.org/doi/10.5555/1190355.1190356

[7] A. Laourine, M.-S. Alouini, S. Affes, and A. Stéphenne, "On the performance analysis of composite multipath/shadowing channels using the G-distribution," *IEEE Trans. Commun.*, vol. 57, no. 4, pp. 1162–1170, Apr. 2009.

[8] P. S. Bithas, A. G. Kanatas, and D. W. Matolak, "Exploiting shadowing stationarity for antenna selection in V2V communications," *IEEE Trans. Veh. Technol.*, vol. 68, no. 2, pp. 1607–1615, Feb. 2019.

[9] P. S. Chauhan and S. K. Soni, "Average SEP and channel capacity analysis over generic/IG composite fading channels: A unified approach," *Phys. Commun.*, vol. 34, pp. 9–18, Jun. 2019.

[10] H. Al-Hmood and H. S. Al-Raweshidy, "Unified modeling of composite $\kappa-\mu$/gamma, $\eta-\mu$/gamma, and $\alpha-\mu$/gamma fading channels using a mixture gamma distribution with applications to energy detection," *IEEE Antennas Wireless Propag. Lett.*, vol. 16, pp. 104–108, Apr. 2017.

[11] S. K. Yoo, N. Bhargav, S. L. Cotton, P. C. Sofotasios, M. Matthaiou, M. Valkama, and G. K. Karagiannidis, "The κ-μ/inverse gamma and η-μ/inverse gamma composite fading models: Fundamental statistics and empirical validation," *IEEE Trans. Commun.*, early access, Dec. 6, 2017, doi: 10.1109/TCOMM.2017.2780110.

[12] S. K. Yoo, S. L. Cotton, P. C. Sofotasios, M. Matthaiou, M. Valkama, and G. K. Karagiannidis, "The Fisher–Snedecor $\mathcal{F}$ distribution: A simple and accurate composite fading model," *IEEE Commun. Lett.*, vol. 21, no. 7, pp. 1661–1664, Jul. 2017.

[13] O. S. Badarneh, D. B. da Costa, P. C. Sofotasios, S. Muhaidat, and S. L. Cotton, "On the sum of Fisher–Snedecor $\mathcal{F}$ variates and its application to maximal-ratio combining," *IEEE Wireless Commun. Lett.*, vol. 7, no. 6, pp. 966–969, Dec. 2018.

[14] L. Kong and G. Kaddoum, "On physical layer security over the Fisher–Snedecor $\mathcal{F}$ wiretap fading channels," *IEEE Access*, vol. 6, pp. 39466–39472, 2018.

[15] S. K. Yoo, P. C. Sofotasios, S. L. Cotton, S. Muhaidat, F. J. Lopez-Martinez, J. M. Romero-Jerez, and G. K. Karagiannidis, "A comprehensive analysis of the achievable channel capacity in $\mathcal{F}$ composite fading channels," *IEEE Access*, vol. 7, pp. 34078–34094, 2019.

[16] S. K. Yoo, P. C. Sofotasios, S. L. Cotton, S. Muhaidat, O. S. Badarneh, and G. K. Karagiannidis, "Entropy and energy detection-based spectrum sensing over $\mathcal{F}$-composite fading channels," *IEEE Trans. Commun.*, vol. 67, no. 7, pp. 4641–4653, Jul. 2019.

[17] H. Al-Hmood and H. S. Al-Raweshidy, "Selection combining scheme over non-identically distributed Fisher–Snedecor $\mathcal{F}$ fading channels," 2019, *arXiv:1905.05595*. [Online]. Available: http://arxiv.org/abs/1905.05595

[18] H. Zhao, L. Yang, A. S. Salem, and M.-S. Alouini, "Ergodic capacity under power adaption over Fisher–Snedecor $\mathcal{F}$ fading channels," *IEEE Commun. Lett.*, vol. 23, no. 3, pp. 546–549, Mar. 2019.

[19] S. Chen, J. Zhang, G. K. Karagiannidis, and B. Ai, "Effective rate of MISO systems over Fisher–Snedecor $\mathcal{F}$ fading channels," *IEEE Commun. Lett.*, vol. 22, no. 12, pp. 2619–2622, Dec. 2018.

[20] T. Aldalgamouni, M. C. Ilter, O. S. Badarneh, and H. Yanikomeroglu, "Performance analysis of Fisher–Snedecor $\mathcal{F}$ composite fading channels," in *Proc. IEEE Middle East North Afr. Commun. Conf.*, Jounieh, Lebanon, Apr. 2018, pp. 1–5.

[21] H. Du, J. Zhang, J. Cheng, and B. Ai, "Sum of Fisher–Snedecor $\mathcal{F}$ random variables and its applications," *IEEE Open J. Commun. Soc.*, vol. 1, pp. 342–356, 2020, doi: 10.1109/OJCOMS.2020.2982770.

[22] H. Du, J. Zhang, K. P. Peppas, H. Zhao, B. Ai, and X. Zhang, "On the distribution of the ratio of products of Fisher–Snedecor $\mathcal{F}$ random variables and its applications," *IEEE Trans. Veh. Technol.*, vol. 69, no. 2, pp. 1855–1866, Feb. 2020.

[23] J. Reig, L. Rubio, and N. Cardona, "Bivariate Nakagami-m distribution with arbitrary fading parameters," *Electron. Lett.*, vol. 38, no. 25, pp. 1715–1717, Dec. 2002.

[24] N. C. Sagias and G. K. Karagiannidis, "Gaussian class multivariate Weibull distributions: Theory and applications in fading channels," *IEEE Trans. Inf. Theory*, vol. 51, no. 10, pp. 3608–3619, Oct. 2005.

[25] N. Y. Ermolova and O. Tirkkonen, "Bivariate η-μ fading distribution with application to analysis of diversity systems," *IEEE Trans. Wireless Commun.*, vol. 10, no. 10, pp. 3158–3162, Oct. 2011.

[26] R. A. A. de Souza, M. D. Yacoub, and G. S. Rabelo, "Bivariate hoyt (Nakagami-q) distribution," *IEEE Trans. Commun.*, vol. 60, no. 3, pp. 714–723, Mar. 2012.

[27] M. A. G. Villavicencio, R. A. A. de Souza, G. C. de Souza, and M. D. Yacoub, "A bivariate κ-μ distribution," *IEEE Trans. Veh. Technol.*, vol. 65, no. 7, pp. 5737–5743, Jul. 2016.

[28] R. A. A. de Souza and G. C. de Souza, "A bivariate α-κ-μ distribution," in *Proc. IEEE Radio Wireless Symp. (RWS)*, Austin, TX, USA, Jan. 2016, pp. 248–251.

[29] R. Zhang, J. Wei, D. G. Michelson, and V. C. M. Leung, "Outage probability of MRC diversity over correlated shadowed fading channels," *IEEE Wireless Commun. Lett.*, vol. 1, no. 5, pp. 516–519, Oct. 2012.

[30] B. Zhu and J. Cheng, "Asymptotic outage analysis on dual-branch diversity receptions over non-identically distributed correlated Lognormal channels," *IEEE Trans. Commun.*, vol. 67, no. 10, pp. 7126–7138, Oct. 2019.

[31] P. S. Bithas, N. C. Sagias, P. T. Mathiopoulos, S. A. Kotsopoulos, and A. M. Maras, "On the correlated K-distribution with arbitrary fading parameters," *IEEE Signal Process Lett.*, vol. 15, pp. 541–544, Jul. 2008.

[32] P. S. Bithas, N. C. Sagias, and P. T. Mathiopoulos, "The bivariate generalized-K (KG) distribution and its application to diversity receivers," *IEEE Trans. Commun.*, vol. 57, no. 9, pp. 2655–2662, Sep. 2009.

[33] T. S. B. Reddy, R. Subadar, and P. R. Sahu, "Outage probability of selection combiner over exponentially correlated Weibull-gamma fading channels for arbitrary number of branches," in *Proc. Nat. Conf. Commun. (NCC)*, Chennai, India, Jan. 2010, pp. 1–5.

[34] Z. Ni, X. Zhang, X. Liu, and D. Yang, "Bivariate Weibull-gamma composite distribution with arbitrary fading parameters," *Electron. Lett.*, vol. 48, no. 18, pp. 1165–1167, Aug. 2012.
[35] N. M. Sekulović and M. Č. Stefanović, "Performance analysis of system with micro-and macrodiversity reception in correlated gamma shadowed Rician fading channels," *Wireless Pers. Commun.*, vol. 65, no. 1, pp. 143–156, Jul. 2012.
[36] P. S. Bithas, A. G. Kanatas, D. B. da Costa, P. K. Upadhyay, and U. S. Dias, "On the double-generalized gamma statistics and their application to the performance analysis of V2V communications," *IEEE Trans. Commun.*, vol. 66, no. 1, pp. 448–460, Jan. 2018.
[37] I. Trigui, A. Laourine, S. Affes, and A. Stéphenne, "Bivariate g distribution with arbitrary fading parameters," in *Proc. 3rd Int. Conf. Signals, Circuits Syst. (SCS)*, Medenine, Tunisia, Nov. 2009, pp. 1–5.
[38] J. Reig, L. Rubio, and V. M. Rodrigo-Peñarrocha, "On the bivariate Nakagami-Lognormal distribution and its correlation properties," *Int. J. Antennas Propag.*, vol. 2014, pp. 1–8, Aug. 2014.
[39] J. Lopez-Fernandez, J. F. Paris, and E. Martos-Naya, "Bivariate Rician shadowed fading model," *IEEE Trans. Veh. Technol.*, vol. 67, no. 1, pp. 378–384, Jan. 2018.
[40] A. H. El-Bassiouny and M. C. Jones, "A bivariate f distribution with marginals on arbitrary numerator and denominator degrees of freedom, and related bivariate beta and t distributions," *Stat. Methods Appl.*, vol. 18, no. 4, pp. 465–481, Apr. 2009.
[41] W. Cheng, X. Xu, X. Wang, and X. Li, "Bivariate Fisher-Snedecor $\mathcal{F}$ distribution with arbitrary fading parameters," in *Proc. 14th EAI Int. Conf. Testbeds Res. Infrastruct. Develop. Netw. Commun. (Trident Com)*, Changsha, China, Dec. 2019, pp. 107–119.
[42] M. Nakagami, "The M-distribution—A general formula of intensity distribution of rapid fading," in *Statistical Methods in Radio Wave Propagation*. Oxford, U.K.: Pergamon Press, 1960.
[43] I. Gradshteyn and I. Ryzhik, *Table of Integrals, Series, and Products*, 7th ed. New York, NY, USA: Academic, 2007.
[44] Wolfram Research. *MeijerG*. Accessed: Apr. 2020. [Online]. Available: http://functions.wolfram.com/HypergeometricFunctions/MeijerG/
[45] V. S. Adamchik and O. I. Marichev, "The algorithm for calculating integrals of hypergeometric type functions and its realization in REDUCE system," in *Proc. Int. Symp. Symbolic Algebr. Comput. (ISSAC)*, Tokyo, Japan, Aug. 1990, pp. 212–224.
[46] A. Lioumpas, G. Karagiannidis, and A. Iossifides, "Channel quality estimation index (CQEI): A long-term performance metric for fading channels and an application in EGC receivers," *IEEE Trans. Wireless Commun.*, vol. 6, no. 9, pp. 3315–3323, Sep. 2007.
[47] T. H. Nguyen and S. B. Yakubovich, *The Double Mellin–Barnes Type Integrals and Their Applications to Convolution Theory*. Singapore: World Scientific, 1992.
[48] G.-C. Celia, F. J. Canete, and F. Paris Jos, "Capacity of κ-μ shadowed fading channels," *Int. J. Antennas Propag.*, vol. 2014, pp. 1–8, Jul. 2014.
[49] A. M. Mathai, R. K. Saxena, and H. J. Haubold, *The H-Function: Theory and Applications*. New York, NY, USA: Springer, 2009.
[50] F. Yilmaz and M.-S. Alouini, "A unified MGF-based capacity analysis of diversity combiners over generalized fading channels," *IEEE Trans. Commun.*, vol. 60, no. 3, pp. 862–875, Mar. 2012.
[51] S. O. Rice, "Mathematical analysis of random noise," *Bell Syst. Tech. J.*, vol. 24, no. 1, pp. 46–156, Jan. 1945.
[52] F. J. López-Martínez, E. Martos-Naya, J. F. Paris, and U. Fernández-Plazaola, "Higher order statistics of sampled fading channels with applications," *IEEE Trans. Veh. Technol.*, vol. 61, no. 7, pp. 3342–3346, Sep. 2012.
[53] Z. Wang and G. B. Giannakis, "A simple and general parameterization quantifying performance in fading channels," *IEEE Trans. Commun.*, vol. 51, no. 8, pp. 1389–1398, Aug. 2003.
[54] J. Reig, M. A. Martinez-Amoraga, and L. Rubio, "Generation of bivariate Nakagami-m fading envelopes with arbitrary not necessary identical fading parameters," *Wireless Commun. Mobile Comput.*, vol. 7, no. 4, pp. 531–537, Jul. 2007.
[55] H. R. Alhennawi, M. M. H. El Ayadi, M. H. Ismail, and H.-A.-M. Mourad, "Closed-form exact and asymptotic expressions for the symbol error rate and capacity of the-function fading channel," *IEEE Trans. Veh. Technol.*, vol. 65, no. 4, pp. 1957–1974, Apr. 2016.
[56] H. Chergui, M. Benjillali, and M.-S. Alouini, "Rician K-factor-based analysis of XLOS service probability in 5G outdoor ultra-dense networks," *IEEE Wireless Commun. Lett.*, vol. 8, no. 2, pp. 428–431, Apr. 2019.
[57] Wolfram Research. *Beta3*. Accessed: Apr. 2020. [Online]. Available: http://functions.wol-fram.com/GammaBetaErf/Beta3/

WEIJUN CHENG (Member, IEEE) received the M.S. degree in electronics and control engineering from the China University of Mining and Technology, Beijing, China, in 1998, and the Ph.D. degree in telecommunications engineering from the Beijing University of Posts and Telecommunications, Beijing, in 2004. He was a Postdoctoral Research Fellow in electronics engineering with Peking University, Beijing, from 2005 to 2007. From October 2017 to October 2018, he was a Visiting Scholar with the School of Electrical, Computer and Energy Engineering, Arizona State University, AZ, USA, along with Prof. J. Zhang. He is currently an Associate Professor with the School of Information Engineering, Minzu University of China, Beijing. His research interests include wireless communication theory and AI in the IoT.

XIAOTING WANG received the B.S. degree in software engineering from Qingdao University, Qingdao, China, in 2019. She is currently pursuing the M.S. degree in computer science and technology with the Minzu University of China, Beijing, China. Her research interest includes mobile edge computing.